NASA TECHNICAL NOTE

NASA TN D-4314

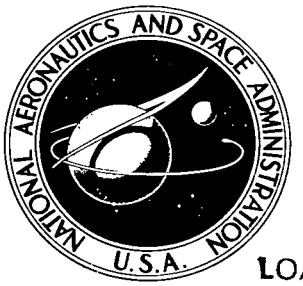

NASA TN D-4314

PRESSURE DISTRIBUTIONS AND AERODYNAMIC CHARACTERISTICS OF 9° AND 15° BLUNTED CONES IN NITROGEN AND HELIUM AT MACH 20

by Theodore R. Creel, Jr., Charles G. Miller III, Dal V. Maddalon, and Ralph D. Watson

Langley Research Center
Langley Station, Hampton, Va.

NATIONAL AERONAUTICS AND SPACE ADMINISTRATION • WASHINGTON, D. C. • MARCH 1968

PRESSURE DISTRIBUTIONS AND AERODYNAMIC CHARACTERISTICS OF 9° AND 15° BLUNTED CONES IN NITROGEN AND HELIUM AT MACH 20

By Theodore R. Creel, Jr., Charles G. Miller III,
Dal V. Maddalon, and Ralph D. Watson

Langley Research Center
Langley Station, Hampton, Va.

NATIONAL AERONAUTICS AND SPACE ADMINISTRATION

For sale by the Clearinghouse for Federal Scientific and Technical Information
Springfield, Virginia 22151 – CFSTI price $3.00

PRESSURE DISTRIBUTIONS AND AERODYNAMIC CHARACTERISTICS OF 9° AND 15° BLUNTED CONES IN NITROGEN AND HELIUM AT MACH 20

By Theodore R. Creel, Jr., Charles G. Miller III,
Dal V. Maddalon, and Ralph D. Watson
Langley Research Center

SUMMARY

An experimental investigation to determine the pressure distributions and force and moment characteristics on a 9° semiapex angle spherically blunted cone was conducted in nitrogen in the Langley hotshot tunnel. Pressure distributions were obtained in the Langley 22-inch helium tunnel on 9° semiapex angle spherically blunted and flat-faced cones and on a 15° semiapex angle spherically blunted cone.

The results of this investigation indicated that pressure distributions on the 9° and 15° semiapex angle spherically blunted cones at zero angle of attack were underpredicted by ideal gas inviscid theory, but a theory accounting for viscous effects predicted the pressure distribution on the 9° spherically blunted cone in nitrogen. Blast-wave-type correlation parameters were observed to yield a fair correlation of pressure distributions obtained on the most windward meridian for angles of attack of 5° to 40° when an effective cone angle was used. Newtonian theory adequately predicted the radial pressure distributions on the windward side of the 9° and 15° semiapex angle spherically blunted cones. The shock shapes of the 9° and 15° cones were correlated by using blast-wave-type correlating parameters. Force and moment coefficients for the 9° spherically blunted cone, for the present investigation, in nitrogen were in good agreement with those of other investigations using air and nitrogen as test gases.

INTRODUCTION

Spherically blunted cones have been the subject of numerous analytical and experimental investigations. One such configuration, a 9° semiapex angle, 0.3 spherically blunted cone, has received extensive testing in a number of wind-tunnel facilities (refs. 1 to 5) and has become regarded as a facility-calibration model. (Bluntness is defined as the ratio of nose radius to base radius.) Cones with other nose geometry and other semiapex angles are of interest from the standpoint of verifying predictions of aerodynamic

characteristics, pressure distribution, shock shapes, and standoff distance. Also of continuing interest is the effect of the flow medium on the characteristics of such configurations.

To provide experimental information for comparison with various theories, correlations, and other experimental data, an investigation of several conical bodies was undertaken in the Langley hotshot tunnel in nitrogen and in the Langley 22-inch helium tunnel. Tests in the hotshot tunnel in nitrogen included force and moment characteristics for the 9° semiapex angle cone along with pressure distributions and shock shapes for angles of attack from 0° to 40° at a Mach number of 20 and a free-stream Reynolds number of approximately 1.4×10^6 per meter. Pressure distributions and shock shape studies in the Langley 22-inch helium tunnel – on the 9° semiapex angle 0.3 spherically blunted cone at zero angle of attack, on the 9° semiapex angle 0.03 flat-face cone at zero angle of attack, and on the 15° semiapex angle 0.15 spherically blunted cone at angles of attack from 0° to 30° – were obtained at a Mach number of 20 and a free-stream Reynolds number of approximately 1.5×10^7 per meter. Data resulting from the present study were compared with the theoretical predictions of reference 6 and to other experimental results.

SYMBOLS

Force and moment coefficients are referred to the body axes and stability axes and are identified in figure 1. The pitching-moment coefficients are referenced to the model nose.

A model base area, πr_b^2

C_A axial-force coefficient, $\dfrac{\text{Axial force}}{q_\infty A}$

C_D drag coefficient, $C_N \sin \alpha + C_A \cos \alpha$

$C_{D,n}$ nose drag coefficient, $\dfrac{\text{Nose drag force}}{q_\infty A}$

C_L lift coefficient, $C_N \cos \alpha - C_A \sin \alpha$

C_m pitching-moment coefficient, $\dfrac{\text{Pitching moment}}{q_\infty A d_b}$

C_N normal-force coefficient, $\dfrac{\text{Normal force}}{q_\infty A}$

C_p	pressure coefficient, $\frac{p_w - p_\infty}{q_\infty}$
d_b	model base diameter
d_n	model nose diameter
L/D	lift-drag ratio, $\frac{C_L}{C_D}$
M_∞	free-stream Mach number
$p_{t,2}$	stagnation pressure behind normal shock
p_w	model surface pressure
p_∞	free-stream static pressure
q_∞	free-stream dynamic pressure
R	free-stream Reynolds number based on diameter of model base
r_b	model base radius
r_n	model nose radius
s	wetted model length measured from model stagnation point at $\alpha = 0$
x	axial coordinate measured from model stagnation point at $\alpha = 0$
z	lateral coordinate measured from model axis, normal to axis
α	angle of attack
γ	ratio of specific heats
θ	cone semiapex angle
ϕ	model circumferential angle measured from the most leeward meridian
ψ	model bluntness ratio, $\frac{r_n}{r_b}$

FACILITIES AND APPARATUS

Tunnels

The present investigation was conducted in the Langley hotshot tunnel and the Langley 22-inch helium tunnel. The Langley hotshot tunnel is a hypervelocity blowdown facility with a run time of approximately 0.1 second. The major components of the tunnel include a capacitor bank, electrical collector, arc chamber, a 10° total-divergence-angle conical nozzle, a 10° cone-cylinder diffuser, and a vacuum chamber and pumps. A more detailed description of the facility, including calibration results, is presented in reference 7.

The Langley 22-inch helium tunnel, with contoured nozzle, is an intermittent closed-cycle blowdown facility with a run time of approximately 1 minute. A more detailed description and calibration of this facility are presented in reference 8.

Models and Tests

The models employed in the present investigation were a 9° semiapex angle spherically blunted ($\psi = 0.3$) cone, a 9° semiapex angle flat-faced ($\psi = 0.03$) cone, and a 15° semiapex angle spherically blunted ($\psi = 0.15$) cone. Sketches of the models, including tabulations of pressure orifice locations, are presented in figure 2.

Forces and moments and pressure distributions obtained on the 9° semiapex angle ($\psi = 0.3$) spherically blunted cone in the Langley hotshot tunnel in nitrogen were obtained at a Mach number of approximately 20 and a free-stream Reynolds number of approximately 1.4×10^6 per meter with a stagnation temperature range of approximately 2500° to 3000° K for angles of attack from 0° to 40°.

Pressure distributions were obtained in the Langley 22-inch helium tunnel on the following models at a Mach number of approximately 20, a free-stream Reynolds number of approximately 1.5×10^7 per meter, and a stagnation temperature of 297° K: a 9° semiapex angle flat-faced ($\psi = 0.03$) cone, a 9° semiapex angle spherically blunted ($\psi = 0.3$) cone, and a 15° semiapex angle spherically blunted ($\psi = 0.15$) cone. The 9° cones were tested only at zero angle of attack and the 15° cone was tested at angles of attack from 0° to 30°.

Single-pass Z-type schlieren systems were used to obtain shock shapes for the present investigation.

Instrumentation

Pressure measurements.- The relatively short test time of the Langley hotshot tunnel (approximately 0.1 second) and low level of model surface pressures to be

measured (approximately 40 to 6895 N/m^2) require pressure transducers having short response times, high sensitivity, and minimum length of orifice tubing. Therefore double-coil single-diaphragm variable-reluctance pressure transducers (ref. 9) were mounted directly in the test model and pitot probe for the hotshot tunnel tests. The maximum inaccuracies in the pressure measurements on the model surface and the pitot probe pressure measurements were believed to be approximately ±15 percent and ±5 percent, respectively. Arc-chamber stagnation pressure was measured by high-response strain-gage transducers having a full-scale rating of 138 MN/m^2. All pressure transducers were excited by 5-volt 20-kilocycle carrier amplifiers. The output signals from the amplifiers drove galvanometers in a light-beam-type oscillograph.

Model surface pressures in the Langley 22-inch helium tunnel were measured by two different types of gages. Pressures greater than 4.0×10^3 N/m^2 were measured by strain-gage diaphragm-type transducers. Diaphragm gages with ratings of 7.0×10^3, 14.0×10^3, and 21.0×10^3 N/m^2 were used to obtain maximum possible accuracy for the ranges of pressures encountered. For pressures less than 4.0×10^3 N/m^2, ionization gages, which employ a radioactive source to ionize the sampled gas, were used. These gages operate on two ranges, 0 to 4.0×10^2 N/m^2 and 0 to 4.0×10^3 N/m^2. Inasmuch as the gages are of the ionization type, they are sensitive to variations in gas composition, being five times more sensitive to air than to helium. For this reason, extreme care was taken to eliminate all possible sources of leaks and outgassing which would result in contamination of the flow thereby producing erroneous data. Maximum inaccuracies of the strain-gage transducers and the ionization gages and errors in the measurements were believed to be approximately 2 percent and 5 percent, respectively.

Force and moment measurements.- An internally mounted strain-gage balance was used to measure forces and moments in the Langley hotshot tunnel. Before each tunnel test the balance was statically calibrated to the anticipated maximum load for the test. Because of the short test time, angle of attack was set before each test and was not changed during the test. Base pressure was not measured during the tests. The maximum uncertainties in the force and moment coefficients as determined from static calibration of the strain-gage balance were as follows:

C_A	±0.02
C_N	±0.02
C_m	±0.01

Data Reduction

A real-nitrogen data-reduction program (ref. 10), using the initial arc-chamber density and the measured values of arc-chamber stagnation pressure and test-section pitot pressure as inputs, was employed to determine test section flow conditions in the Langley hotshot tunnel. The validity of the simplifying assumptions and uncertainties associated with computed flow parameters are discussed in the appendix of reference 7.

Test section flow conditions in the Langley 22-inch helium tunnel were computed by using the ideal-gas relations of reference 11 in conjunction with the real-gas correction factors of reference 12.

RESULTS AND DISCUSSION

Pressure Distributions

9° spherically blunted cone.- Pressure distributions for the 9° semiapex angle spherically blunted ($\psi = 0.3$) cone are shown in figure 3 for angles of attack from 0° to 40°. The ratio of model surface pressure to stagnation pressure behind a normal shock is plotted against the ratio of wetted model surface length to model nose radius s/r_n where negative values of s/r_n correspond to the most windward ray ($\phi = 180^{\circ}$) and positive values of s/r_n correspond to the most leeward ray ($\phi = 0$). Also shown in figure 3 are air (ref. 2) and nitrogen (ref. 5) results obtained in other hypervelocity wind tunnels.

At zero angle of attack (fig. 3(a)), the present nitrogen results and those of references 2 and 5 are observed to be in good agreement and exhibit the common feature of an overexpansion with respect to the Mach 20 sharp cone solution. (Sharp cone solutions were obtained from ref. 13 for air and nitrogen and from ref. 11 for helium.) It should be noted that the results of reference 2 for zero angle of attack have been adjusted so that the pressure ratio at $s/r_n = 0$ is unity. The nitrogen and air surface pressure ratios are slightly less than the Mach 20 helium surface pressure ratios. This effect is believed to be primarily a result of the difference in specific heat ratios between the two gases. The free-stream Reynolds number difference between the helium tests and the nitrogen and air tests (R for the helium tests is greater than for the air and nitrogen tests) is, according to references 14 and 15, in the wrong direction to yield the noted difference. Also shown in figure 3(a) are ideal gas theoretical inviscid predictions using the method of reference 16 for both Mach 20 nitrogen and helium and the theoretical result of reference 17 for Mach 18 air flow which includes viscous effects. The results of reference 17 corresponding to a hypersonic viscous parameter of 0.047 are shown in figure 3(a) of the present study since this value is approximately that of the present nitrogen results as well as those of reference 5. The theoretical viscous solution of reference 17 is

observed, in general, to predict more accurately measured nitrogen and air surface pressure ratios than the inviscid theoretical prediction of reference 16. As with the nitrogen results, the inviscid theoretical prediction of reference 16 for helium underpredicts the present helium surface pressure ratios (fig. 3(a)) and implies that viscous and other second-order effects (as discussed in ref. 17) may contribute approximately 20 percent of the induced helium surface pressure at $s/r_n \approx 11$. For angles of attack of 10^o to 40^o (figs. 3(b) to 3(e)), the present nitrogen pressure distributions and those of reference 2 in air are observed to be in fair agreement. The asymptotic sharp cone solutions (ref. 13) for cone angles corresponding to effective semiapex angles, $\theta + \alpha$, are observed to represent a reasonable estimation of the windward ray pressure ratios.

Radial pressure distributions on the 9^o spherically blunted ($\psi = 0.3$) cone in Mach 20 nitrogen flow are shown in figure 4 for angles of attack of 10^o to 40^o for several s/r_n stations. Newtonian theory ($C_{p,max} = 2$) is observed to give a reasonable estimate of the windward radial pressure distribution to $\alpha = 20^o$ (figs. 4(a) and 4(b)).

9^o flat-faced cone.- The present Mach 20 helium pressure distribution on a 9^o flat-faced ($\psi = 0.03$) cone is compared in figure 5 to the Mach 16 to 19 nitrogen results of reference 5. The nitrogen data of reference 5 show a decay in pressure ratio for $s/r_n > 55$ to a value below the predicted asymptotic sharp cone solution, whereas the helium results show the pressure ratio to remain essentially constant for $s/r_n > 55$ and to be slightly greater than the asymptotic value.

15^o spherically blunted cone.- Pressure distributions on the windward and leeward rays of the 15^o spherically blunted ($\psi = 0.15$) cone for Mach 20.5 helium flow are shown in figure 6 together with the Mach 21 results of reference 18 in nitrogen and the inviscid theoretical predictions of reference 16 for Mach 20 helium and nitrogen. At zero angle of attack (fig. 6(a)), the helium results of this investigation and the nitrogen results of reference 18 are in good agreement, both sets of data illustrating an overexpansion and recompression to the Mach 20 sharp cone solutions occurring within the measured s/r_n range. The inviscid theoretical predictions of reference 16 are observed to underpredict the measured pressure ratios in the overexpansion-recompression region at zero angle of attack. The present helium pressure distributions and the nitrogen pressure distributions of reference 18 are observed to be in good agreement to 15^o angle of attack (see figs. 6(b) to (d)). As with the 9^o spherically blunted cone, the asymptotic sharp cone solutions for the 15^o cone for effective semiapex angles, $\theta + \alpha$, represent a good approximation of the windward surface pressure ratios at all angles of attack.

Mach 20.5 helium of the present investigation and Mach 21 nitrogen (ref. 18) radial pressure distributions for the 15^o spherically blunted cone are shown in figure 7 for angles of attack from 5^o to 30^o. The two sets of data are observed to be in good agreement on the windward surface for all angles of attack and also on the leeward surface for

angles of attack to 15°. Newtonian theory adequately predicts the windward circumferential pressure distributions for the range of angle of attack tested.

Correlations of Pressure Distributions

Results from the 9° spherically blunted and flat-faced cones of the present investigation and of references 2 and 5, and the results from the 15° spherically blunted cone of the present investigation and of reference 18, are shown in figure 8 in terms of the theoretical blast-wave-type correlating parameters derived in reference 6. For zero angle of attack (fig. 8(a)), the theoretical results of reference 6 are observed to be in reasonable agreement with the experimental data to $\frac{\theta^2}{\sqrt{C_{D,n}}} \frac{x}{d_n} \approx 0.07$ radian^2. As the theory of reference 6 is limited to small values of $\frac{\theta^2}{\sqrt{C_{D,n}}} \frac{x}{d_n}$, it would not be expected to predict the experimental overexpansion-recompression region. However, the pressure distributions are observed to correlate reasonably well.

In an attempt to correlate the most windward pressure distributions for the 9° spherically blunted and flat-faced cones with those of the 15° spherically blunted cones at angles of attack from 5° to 40°, the correlating parameters of reference 6 were employed with effective cone semiapex angles, $\theta + \alpha$, as shown in figure 8(b). The data are observed to correlate reasonably well.

Shock Shapes

Representative schlieren photographs illustrating shock shapes obtained on the cones of this investigation in nitrogen and helium at a Mach number of approximately 20 and zero angle of attack are shown in figure 9. The shock coordinates for the 9° spherically blunted cone for nitrogen and helium are presented in figure 10, where the shock coordinates are nondimensionalized by the model nose radius. As expected, the shock displacement from the model surface for Mach 20.5 helium is greater than the shock displacement for Mach 20 nitrogen. Also shown in figure 10 are ideal-gas inviscid shock shapes predicted from the method of reference 16 for both Mach 20 nitrogen and helium. The theoretical predictions of reference 16 for both nitrogen and helium are observed to be in reasonably good agreement with measured shock displacement.

The shock-wave shapes for the 9° and 15° cones at zero angle of attack are shown in figure 11 in terms of the blast-wave-type correlating parameters derived in reference 6. Also shown in this figure are the experimental results of reference 5 and the theoretical results of references 6 and 19 (correlating parameters of ref. 19 are similar to those of ref. 6). The theoretical results of reference 6 are based on hypersonic

slender-body theory while those of reference 19 were obtained, independently, from blast-wave analogies. The predictions of references 6 and 19 are observed to underestimate the measured shock displacements of the present study and those of reference 5. For a given value of γ, the results of reference 6 predict a greater shock displacement than those of reference 19, and hence are in better agreement with the measured values for $\frac{\theta^2}{\sqrt{C_{D,n}}} \frac{x}{d_n} < 0.5$ radian^2. Reference 19 predicts that the shock waves become conical at $\frac{\theta^2}{\sqrt{C_{D,n}}} \frac{x}{d_n} \approx 0.5$ radian^2 and thus predicts the trends of both the present results and those of reference 5 for the 9° flat-faced and 15° spherically blunted cones. The theory of reference 6 is restricted to small values of x/d_n and therefore is not applicable in the region where the shock wave becomes conical.

Longitudinal Aerodynamic Characteristics

The longitudinal aerodynamic characteristics of the 9° spherically blunted ($\psi = 0.3$) cone obtained in the present investigation are compared in figure 12 with data from other investigations (refs. 1 and 2).

As can be seen in figure 12, the aerodynamic characteristics of the present investigation are in good agreement with the data from references 1 and 2.

CONCLUSIONS

An experimental investigation to determine the pressure distributions and force and moment characteristics on a 9° semiapex angle spherically blunted cone was conducted in nitrogen in the Langley hotshot tunnel together with pressure distributions in the Langley 22-inch helium tunnel on 9° semiapex angle spherically blunted and flat-faced cones and on a 15° semiapex angle spherically blunted cone. The analysis of the results of the present investigation and comparison with the results of other investigations have yielded the following conclusions:

1. Pressure distributions on the 9° and 15° cones in nitrogen and helium were in agreement. Although inviscid theory underpredicted pressure distributions on the 9° and 15° semiapex angle spherically blunted cones, theory accounting for viscous effects predicted the pressure distributions on the 9° spherically blunted cone in nitrogen. Newtonian theory adequately predicted radial pressure distributions on the windward side of 9° and 15° spherically blunted cones.

2. Blast-wave-type correlation parameters were observed to yield a fair correlation of pressure distributions obtained on the most windward meridian for angles of attack of 5° to 40° when an effective cone angle was used.

3. Shock shapes for the 9° and 15° cones correlated well when blast-wave-type correlating parameters were used.

4. The aerodynamic characteristics obtained on the 9° spherically blunted cone in the present investigation in nitrogen were in good agreement with those of other investigations in other facilities.

Langley Research Center,
National Aeronautics and Space Administration,
Langley Station, Hampton, Va., August 1, 1967,
124-07-02-54-23.

REFERENCES

1. Edenfield, E. E.: Comparison of Hotshot Tunnel Force, Pressure, Heat-Transfer and Shock Shape Data With Shock Tunnel Data. AEDC-TDR-64-1, U.S. Air Force, Jan. 1964.

2. Wilkinson, David B.; and Harrington, Shelby A.: Hypersonic Force, Pressure, and Heat Transfer Investigations of Sharp and Blunt Slender Cones. AEDC-TDR-63-177, U.S. Air Force, Aug. 1963.

3. Whitfield, Jack D.; and Griffith, B. J.: Viscous Effects on Zero-Lift Drag of Slender Blunt Cones. AEDC-TDR-63-35, U.S. Air Force, Mar. 1963.

4. Whitfield, Jack D.; and Wolny, W.: Hypersonic Static Stability of Blunt Slender Cones. AEDC-TDR-62-166, U.S. Air Force, Aug. 1962.

5. Lewis, Clark H.: Pressure Distribution and Shock Shape Over Blunted Slender Cones at Mach Numbers From 16 to 19. AEDC-TN-61-81, U.S. Air Force, Aug. 1961.

6. Mirels, Harold; and Thornton, Philip R.: Effect of Body Perturbations on Hypersonic Flow Over Slender Power Law Bodies. NASA TR R-45, 1959.

7. Miller, Charles G., III; Creel, Theodore R., Jr.; and Smith, Fred M.: Calibration Experience in the Langley Hotshot Tunnel for Mach Numbers from 12 to 26. NASA TN D-3278, 1966.

8. Arrington, James P.; Joiner, Roy C., Jr.; and Henderson, Arthur, Jr.: Longitudinal Characteristics of Several Configurations at Hypersonic Mach Numbers in Conical and Contoured Nozzles. NASA TN D-2489, 1964.

9. Smotherman, W. E.; and Maddox, W. V.: Variable Reluctance Pressure Transducer Development. AEDC-TDR-63-135, U.S. Air Force, July 1963.

10. Grabau, Martin; Humphry, Richard L.; and Little, Wanda J.: Determination of Test-Section, After-Shock, and Stagnation Conditions in Hotshot Tunnels Using Real Nitrogen at Temperatures From 3000 to 4000^{o} K. AEDC-TN-61-82, U.S. Air Force, July 1961.

11. Mueller, James N.: Equations, Tables, and Figures for Use in the Analysis of Helium Flow at Supersonic and Hypersonic Speeds. NACA TN 4063, 1957.

12. Erickson, Wayne D.: Real-Gas Correction Factors for Hypersonic Flow Parameters in Helium. NASA TN D-462, 1960.

13. Bertram, Mitchel H.: Correlation Graphs for Supersonic Flow Around Right Circular Cones at Zero Yaw in Air as a Perfect Gas. NASA TN D-2339, 1964.

14. Wagner, Richard D., Jr.; and Watson, Ralph: Induced Pressures and Shock Shapes on Blunt Cones in Hypersonic Flow. NASA TN D-2182, 1964.

15. Wagner, Richard D., Jr.; and Watson, Ralph: Reynolds Number Effects on the Induced Pressures of Cylindrical Bodies With Different Nose Shapes and Nose Drag Coefficients in Helium at a Mach Number of 24. NASA TR R-182, 1963.

16. Lomax, Harvard; and Inouye, Mamoru: Numerical Analysis of Flow Properties About Blunt Bodies Moving at Supersonic Speeds in an Equilibrium Gas. NASA TR R-204, 1964.

17. Lewis, Clark H.; and Whitfield, Jack D.: Theoretical and Experimental Studies of Hypersonic Viscous Effects. AEDC-TR-65-100, May 1965.

18. Martellucci, Anthony; and Seidman, Mitchell: Pressure Distribution at a Mach Number of 21 for a Blunted 15° Circular Cone. Tech. Rept. No. 187 (Contract No. AF 33(616)-6692), Gen Appl. Sci. Lab., Inc., Nov. 8, 1960. (Available from DDC as AD 323 145.)

19. Cheng, Hsien K.: Hypersonic Flow With Combined Leading-Edge Bluntness and Boundary-Layer Displacement Effect. Rept. No. AF-1285-A-4 (Contract Nonr-2653(00)), Cornell Aero. Lab., Inc., Aug. 1960.

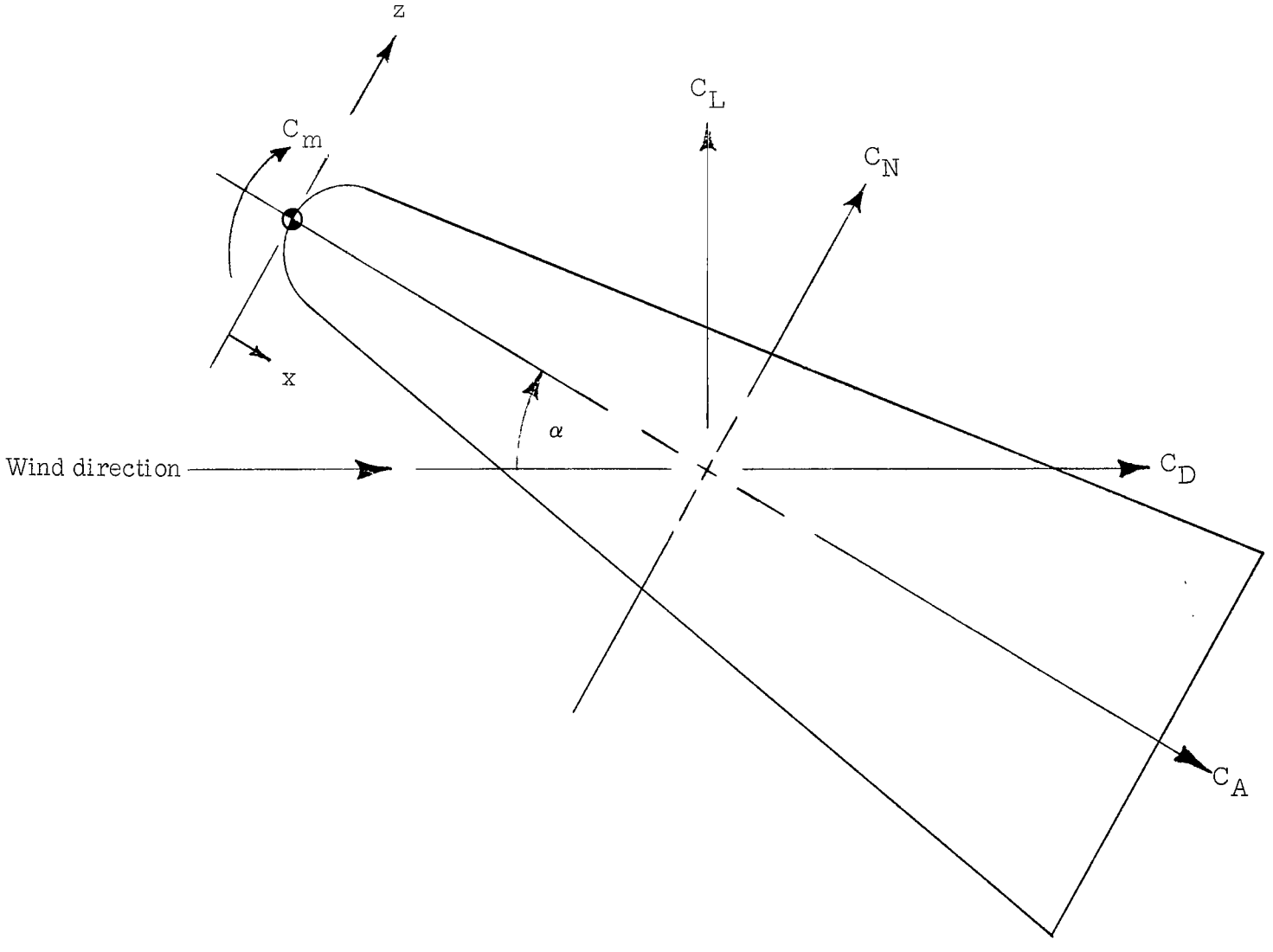

Figure 1.- Sketch showing positive direction of force and moment coefficients and angle of attack for the present investigation.

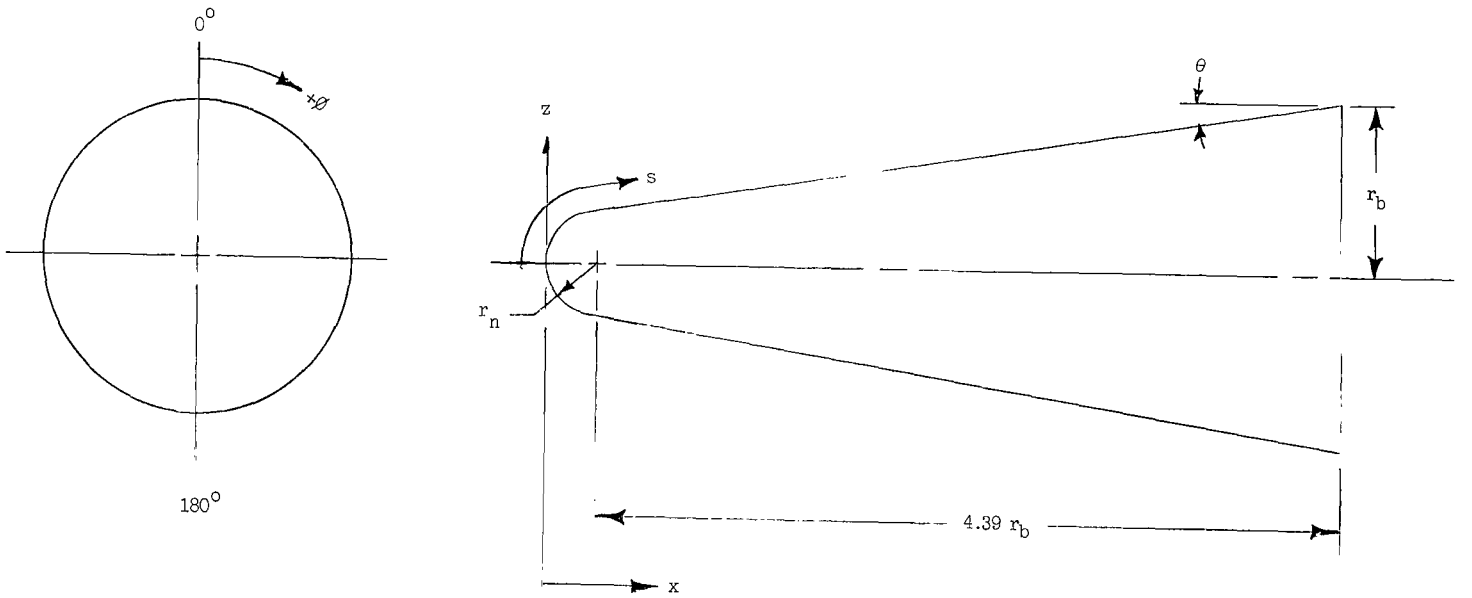

Pressure orifice location

Hotshot tunnel model		22-inch helium tunnel model	
$\lvert s/r_n \rvert$	Ø, deg	$\lvert s/r_n \rvert$	Ø, deg
0	0	0	0
1.4	0, 180	.5	180
3.6	0, ±90, 180	1.0	↓
5.9	0, 180	1.5	↓
8.1	0, 45, ±90, ±135, 180	2.0	↓
10.3	0, 180	3.0	↓
12.5	0, 180	4.0	↓
14.8	0, ±90, ±135, 180	5.0	↓
		6.0	↓
		7.0	↓
		8.0	↓
		9.0	↓
		10.0	↓
		11.0	↓

(a) 9^0 spherically blunted cone; $\psi = 0.3$; $r_b = 3.81$ cm.

Figure 2.- Sketches of models illustrating geometry and instrumentation location.

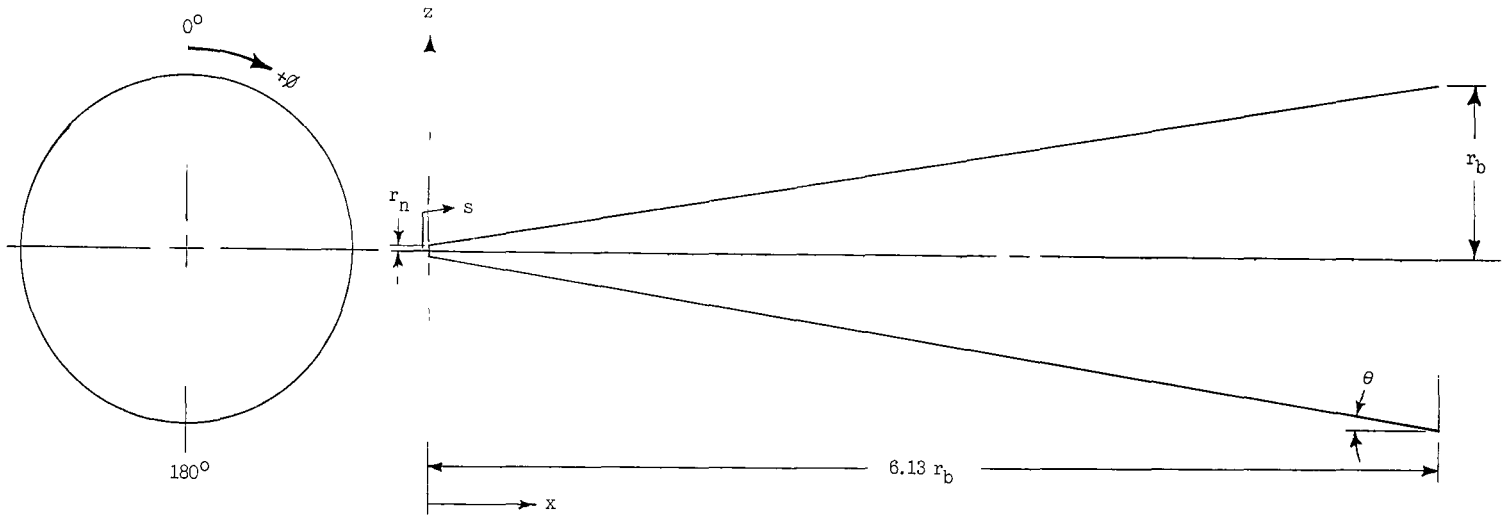

Pressure orifice location

s/r_n	ø, deg	s/r_n	ø, deg
		70	-90
		80	180
35	180	90	180
40	-90	110	180
45	180	130	180
50	-90	150	180
55	180		
60	-90	190	180
65	180	200	180

(b) 9^0 flat-faced cone; $\psi = 0.03$; $r_b = 3.81$ cm.

Figure 2.- Continued.

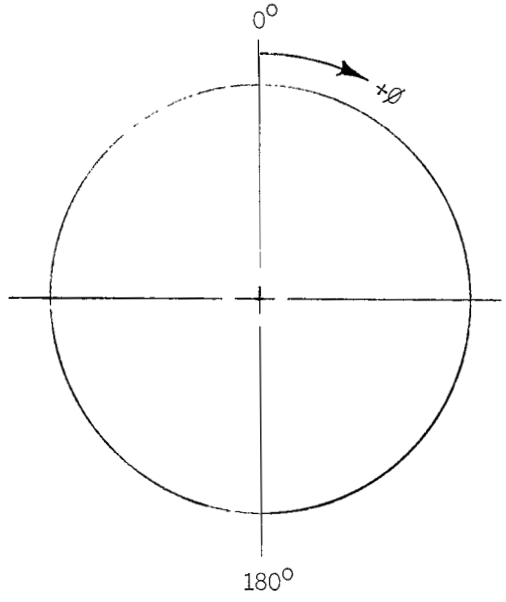

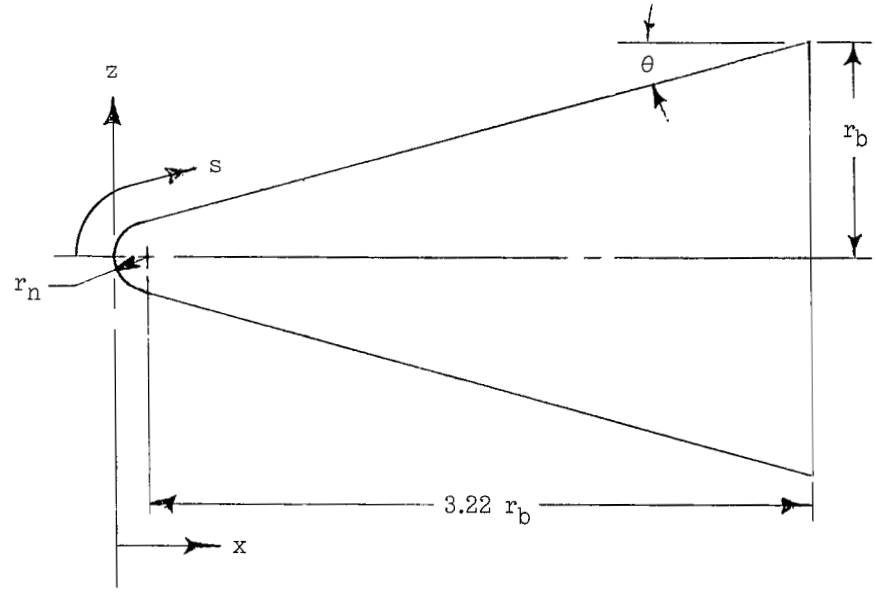

Pressure orifice location	
s/r_n	ø, deg
0	0
.70	0, 180
1.22	0, 180
1.98	0, 180
3.47	0, 90, 180
6.41	0, 180
10.48	0, 180
14.48	0, -60, -90, 90, 120, 180
19.32	0, -90, 180, 90

(c) 15^0 spherically blunted cone; $\psi = 0.15$; $r_b = 3.81$ cm.

Figure 2.- Concluded.

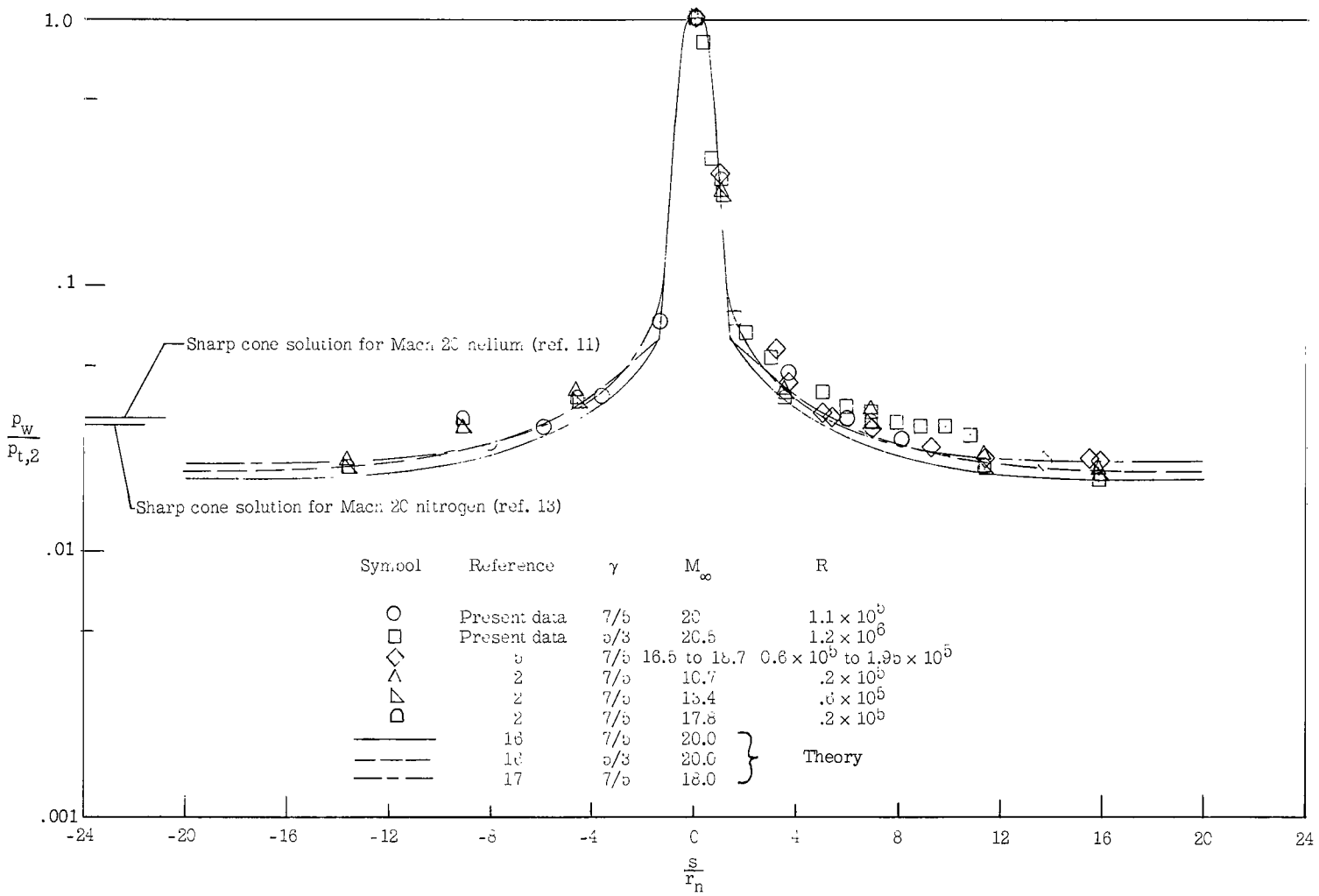

(a) $\alpha = 0^0$.

Figure 3.- Pressure distribution at angles of attack for a 9^0 semiapex angle spherically blunted cone. $\psi = 0.3$.

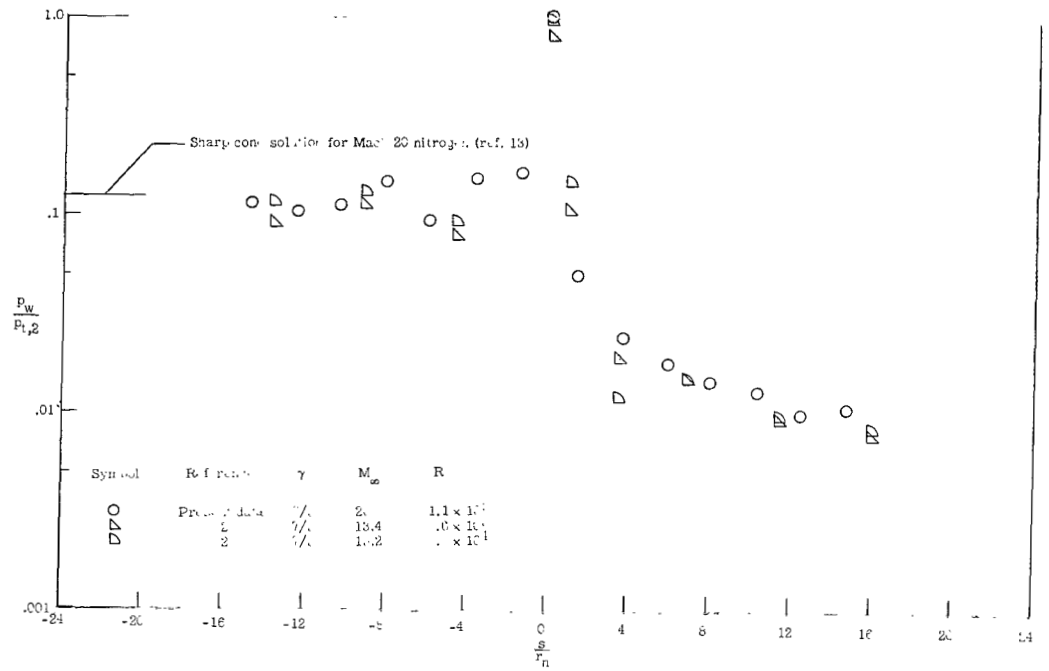

(b) $\alpha = 10^0$.

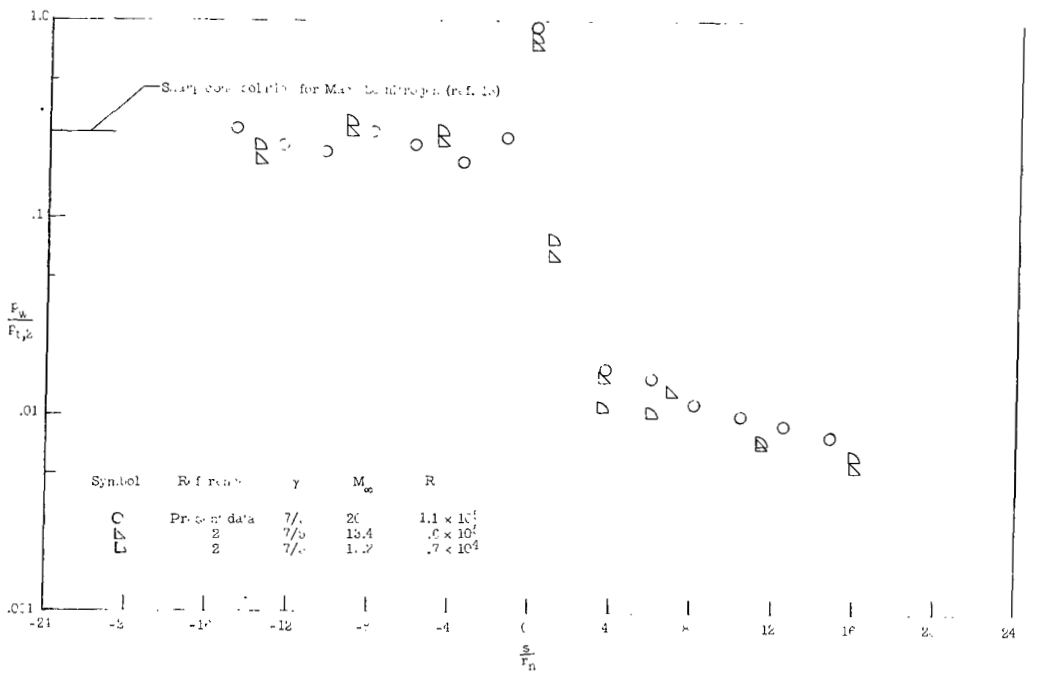

(c) $\alpha = 20^0$.

Figure 3.- Continued.

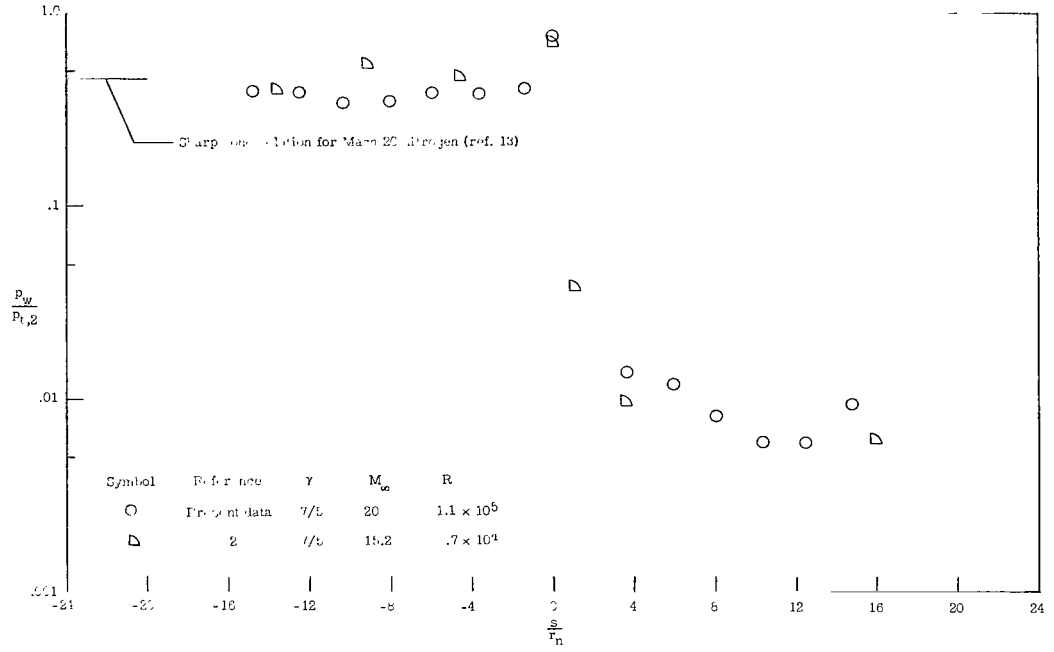

(d) $\alpha = 30^0$.

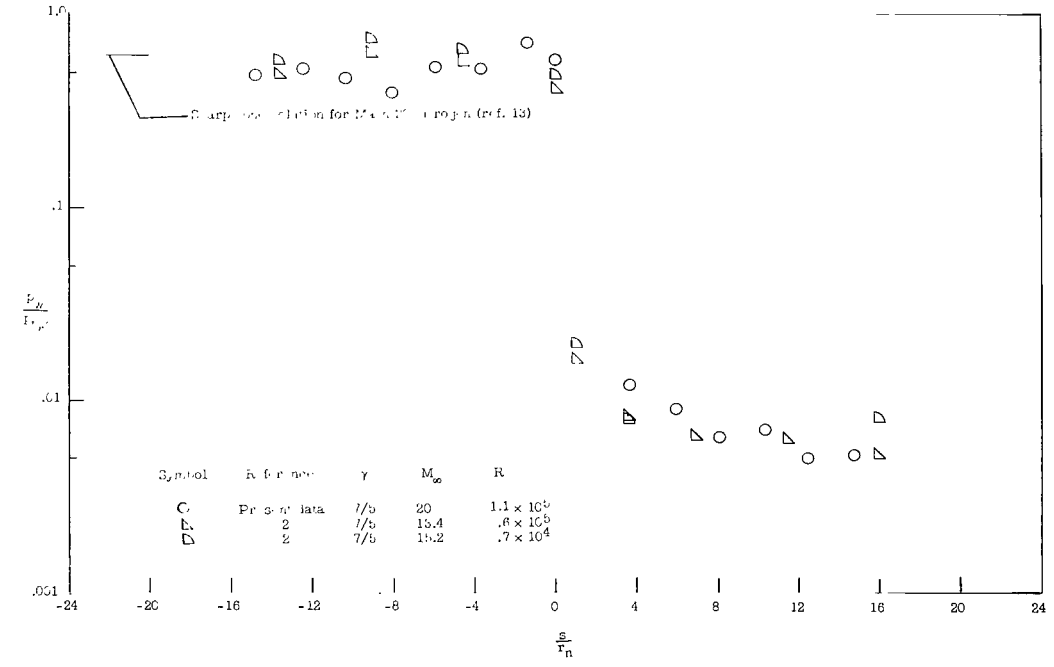

(e) $\alpha = 40^0$.

Figure 3.- Concluded.

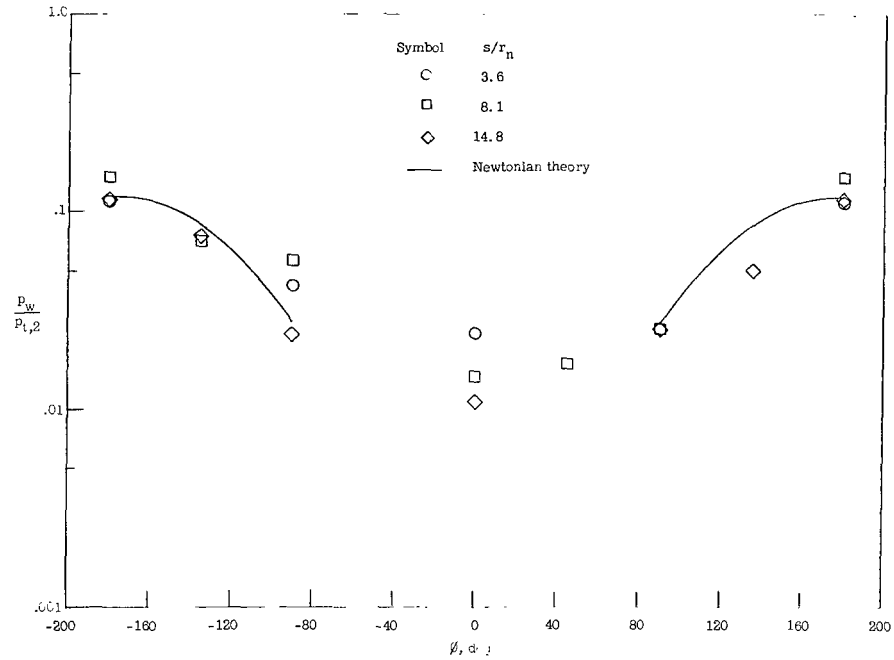

(a) $\alpha = 10^0$.

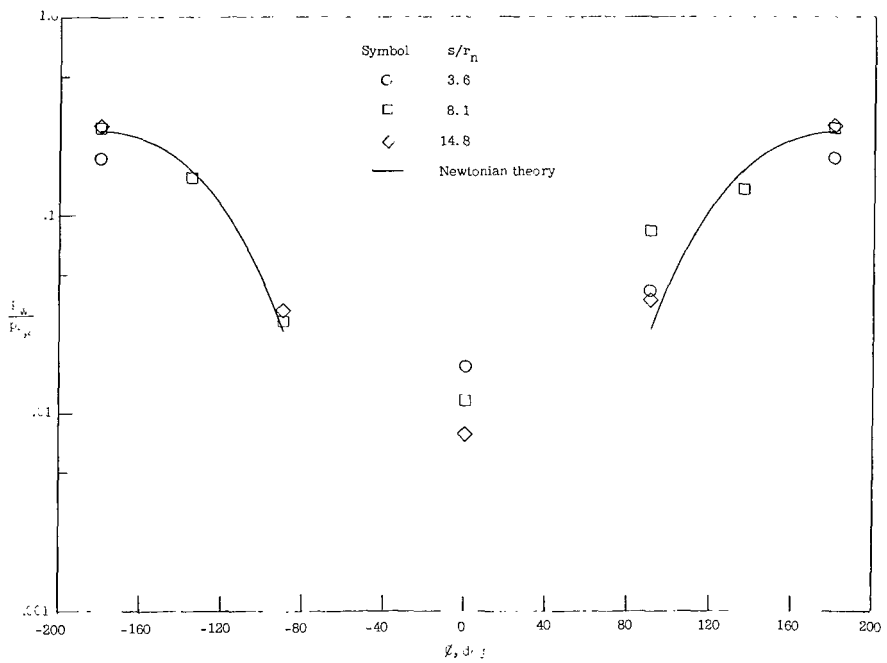

(b) $\alpha = 20^0$.

Figure 4.- Radial pressure distributions at angles of attack for a 9^0 spherically blunted cone at $M_\infty \approx 20$ and $\gamma = 7/5$. $\psi = 0.3$; $R \approx 1.1 \times 10^5$.

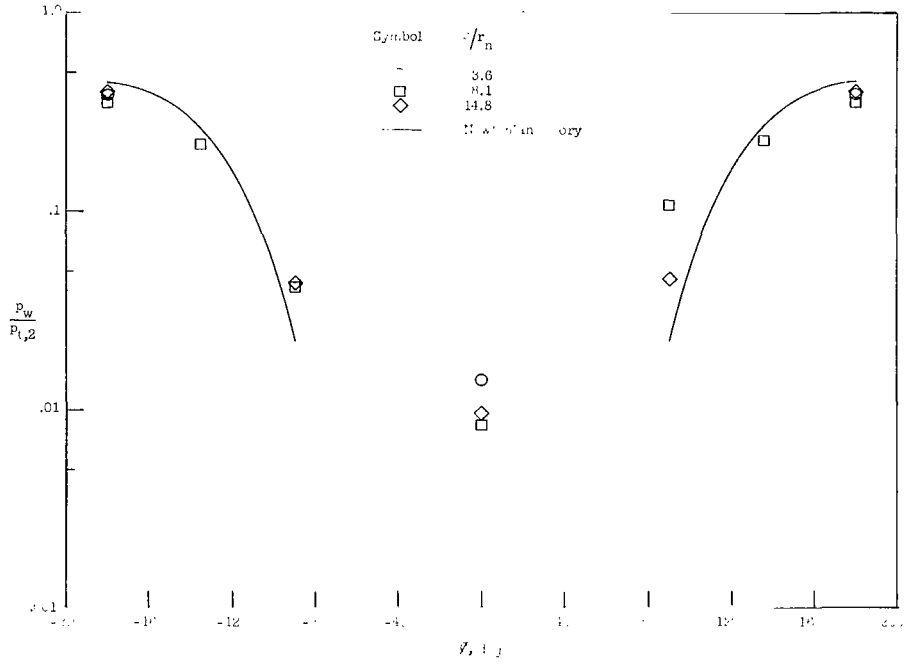

(c) $\alpha = 30^0$.

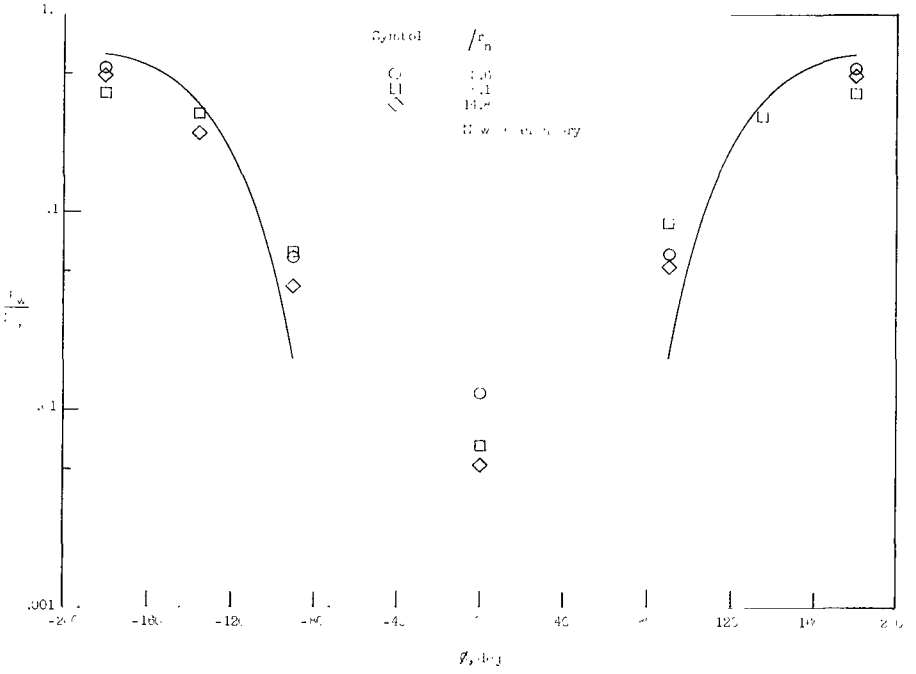

(d) $\alpha = 40^0$.

Figure 4.- Concluded.

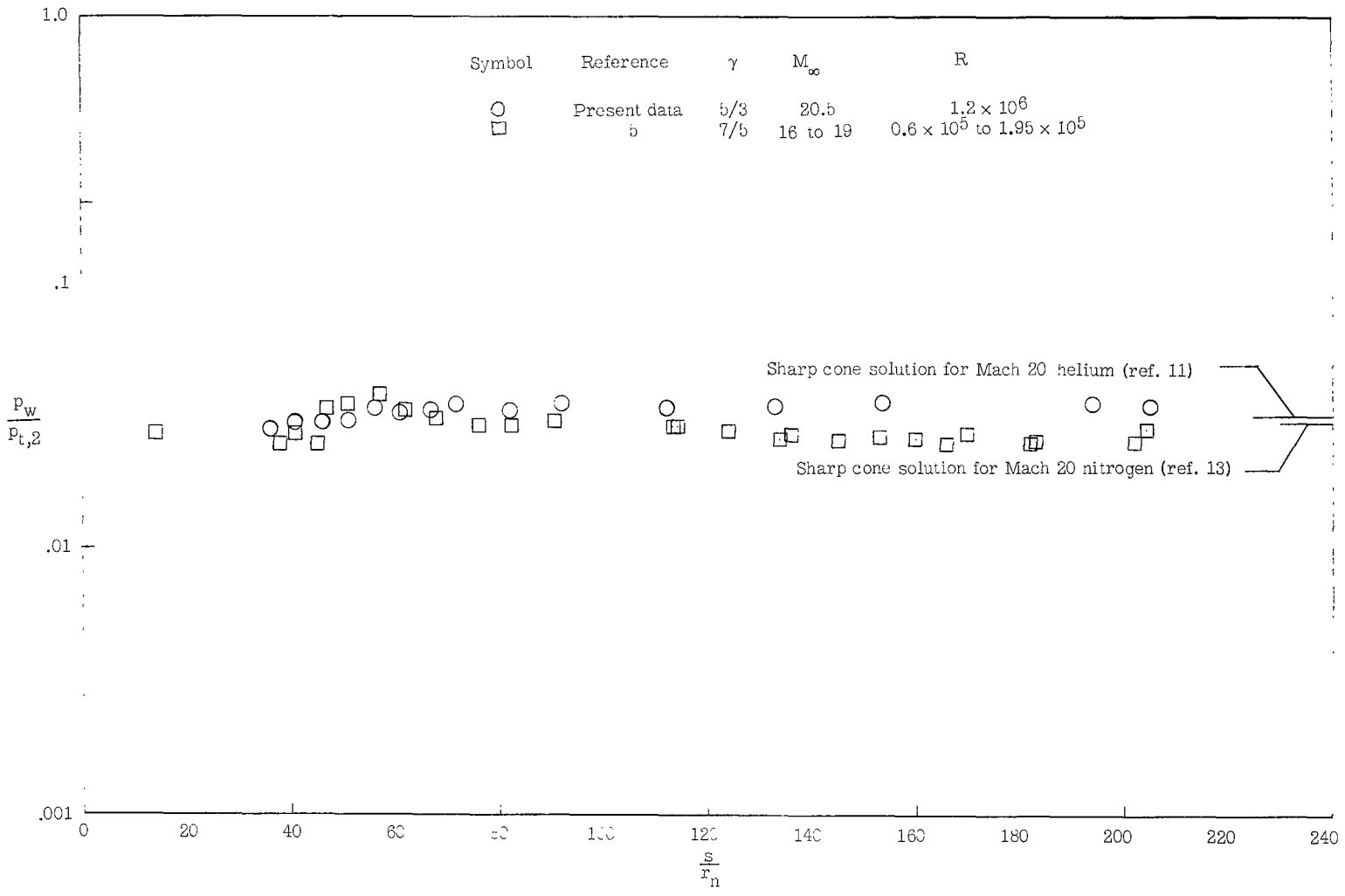

Figure 5.- Pressure distribution on a 9° flat-faced cone for $\alpha = 0^0$. $\psi = 0.03$.

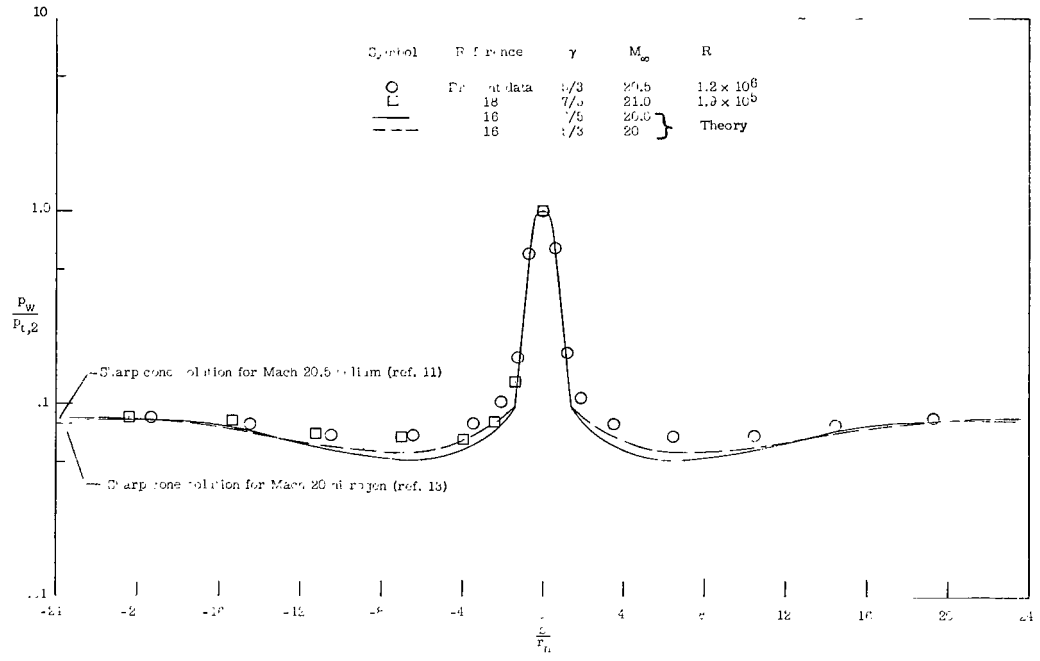

(a) $\alpha = 0^0$.

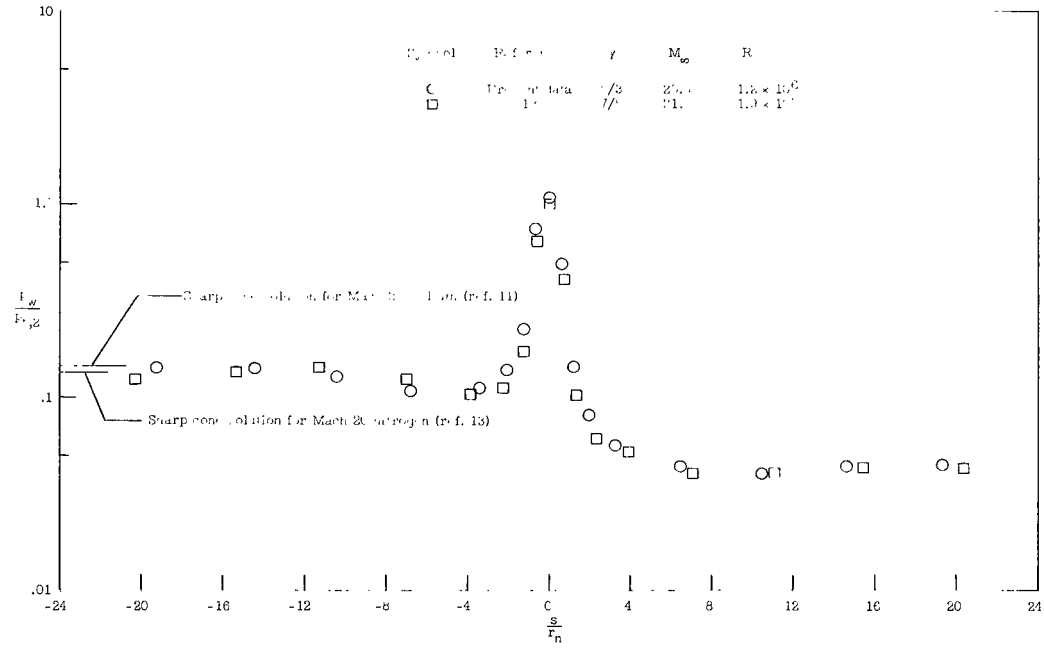

(b) $\alpha = 5^0$.

Figure 6.- Pressure distributions at angles of attack for a 15^0 spherically blunted cone. $\psi = 0.15$.

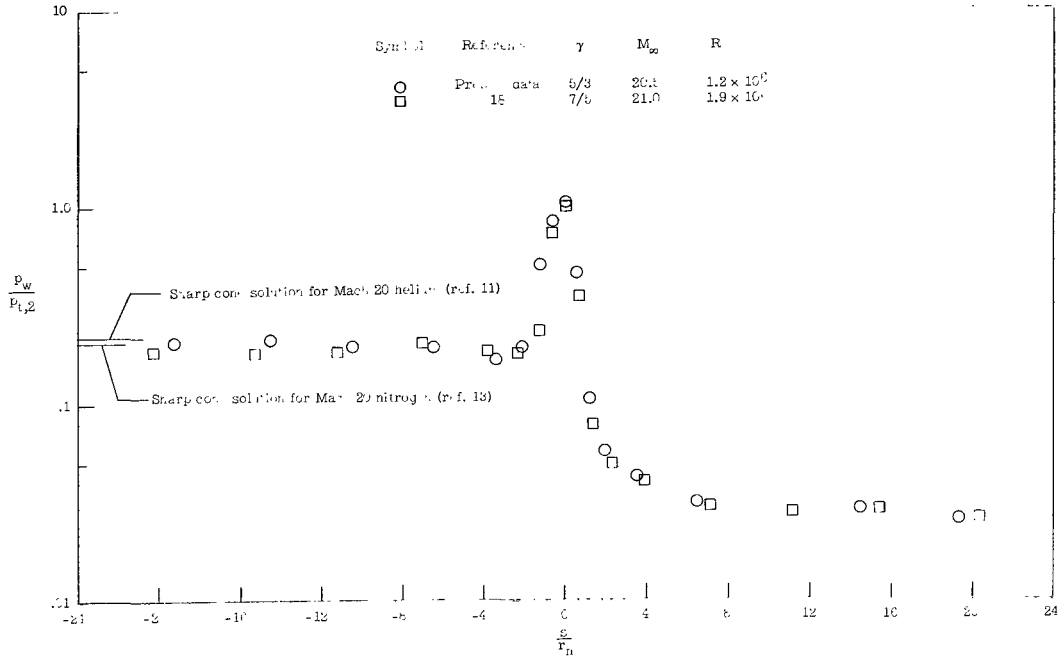

(c) $\alpha = 10^0$.

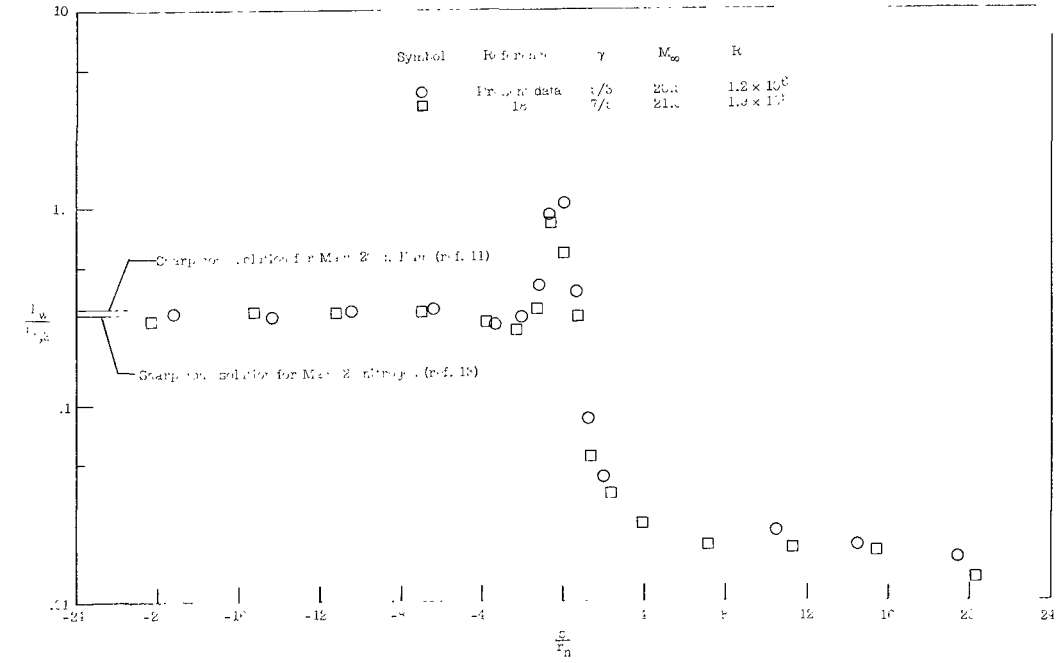

(d) $\alpha = 15^0$.

Figure 6.- Continued.

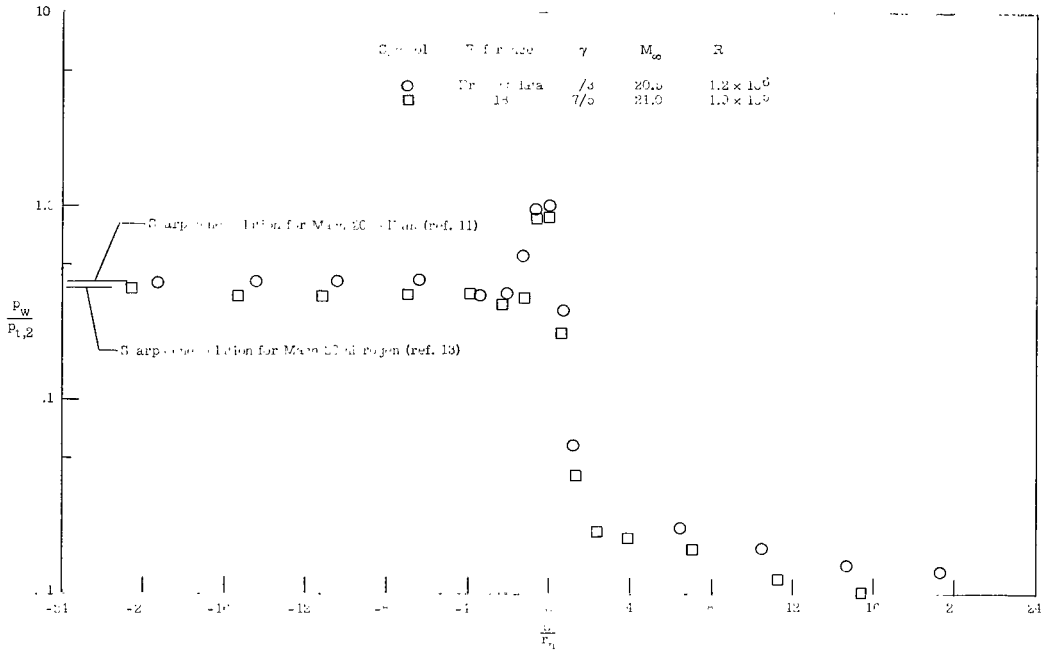

(e) $\alpha = 20^{0}$.

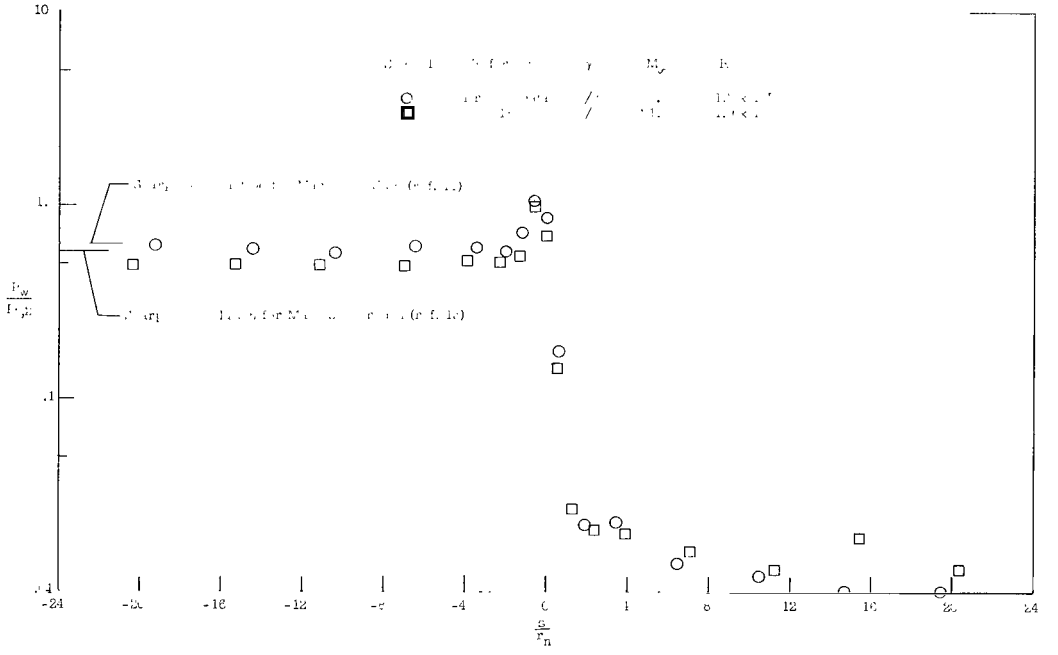

(f) $\alpha = 30^{0}$.

Figure 6.- Concluded.

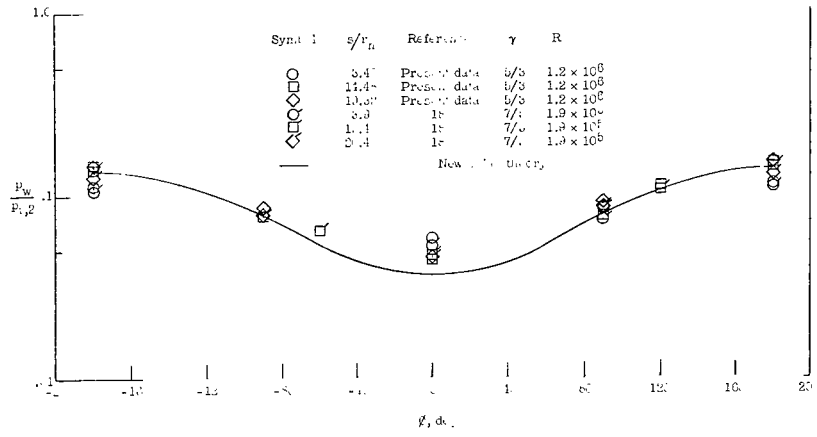

(a) $\alpha = 5^0$.

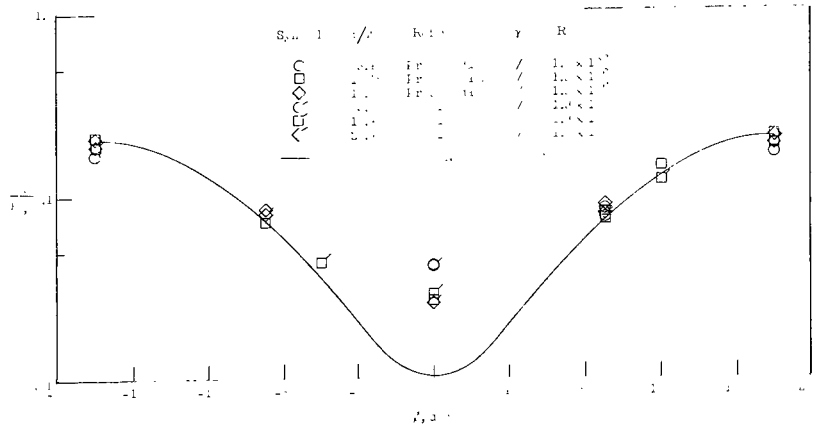

(b) $\alpha = 10^0$.

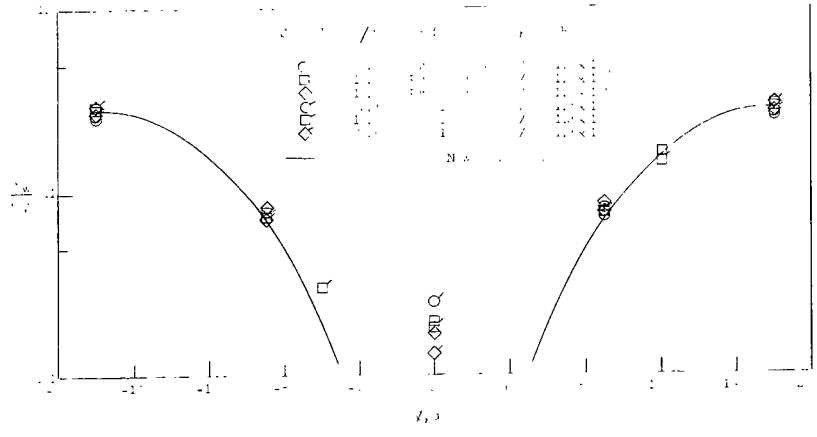

(c) $\alpha = 15^0$.

Figure 7.- Radial pressure distributions on a 15^0 spherically blunted cone at $M_\infty \approx 21$ for various angles of attack. $\psi = 0.15$.

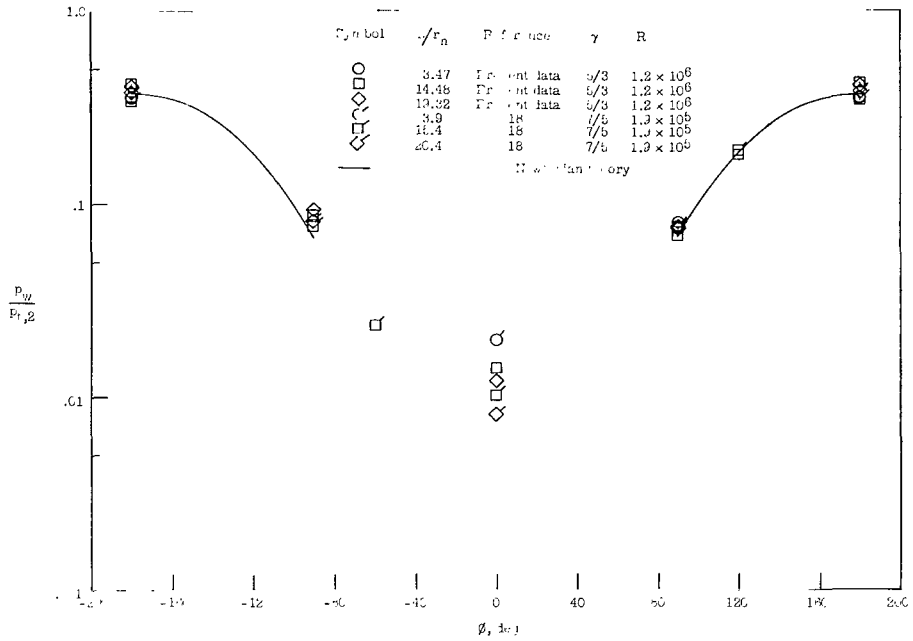

(d) $\alpha = 20^0$.

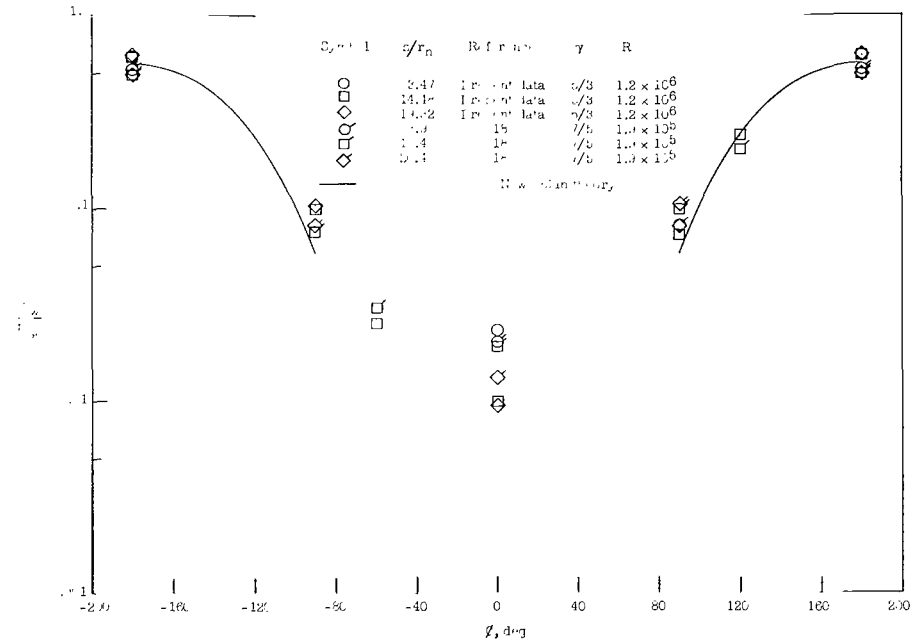

(e) $\alpha = 30^0$.

Figure 7.- Concluded.

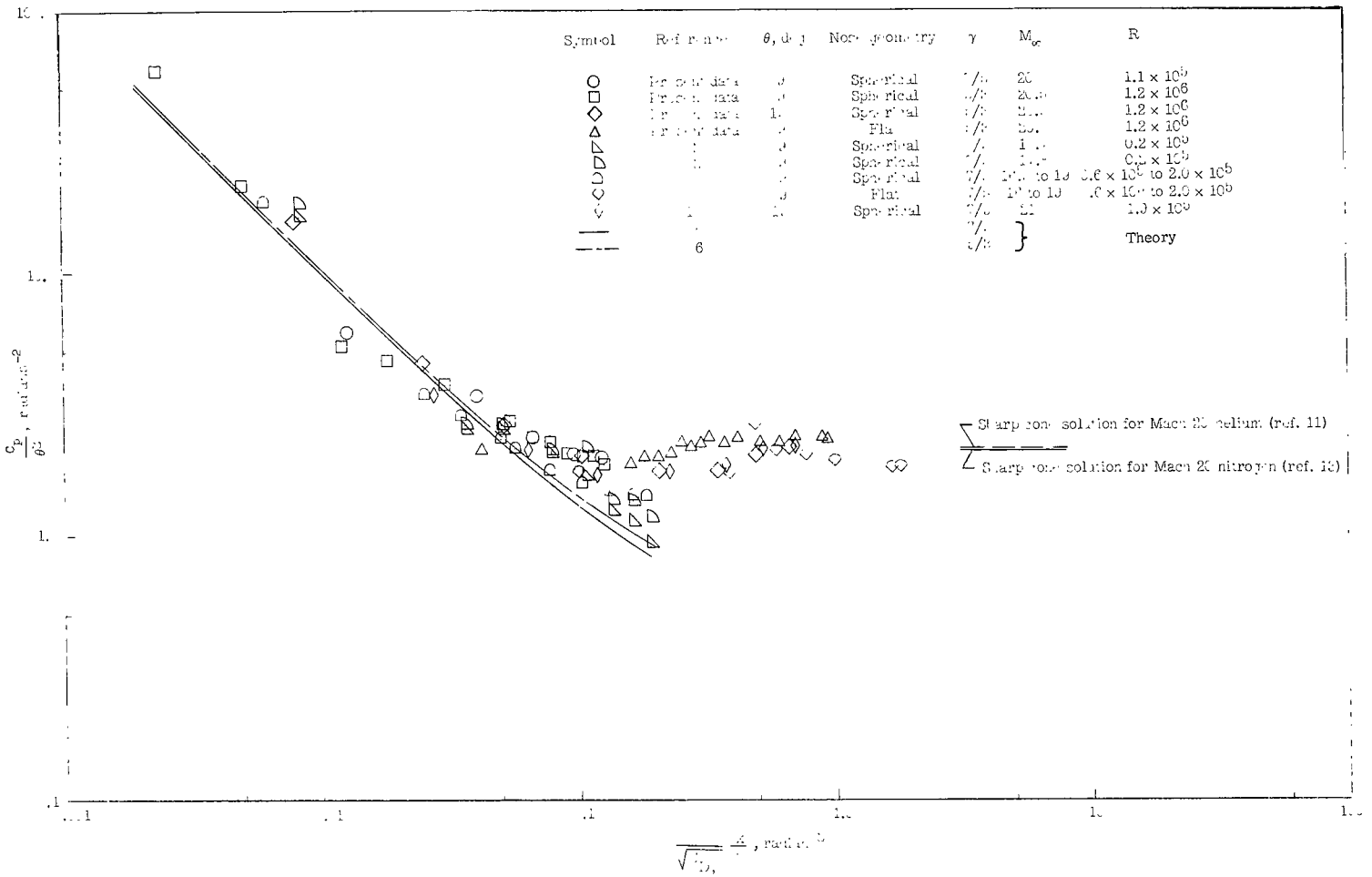

(a) $\alpha = 0^0$.

Figure 8.- Correlation of pressure distributions on 9^0 and 15^0 blunted cones.

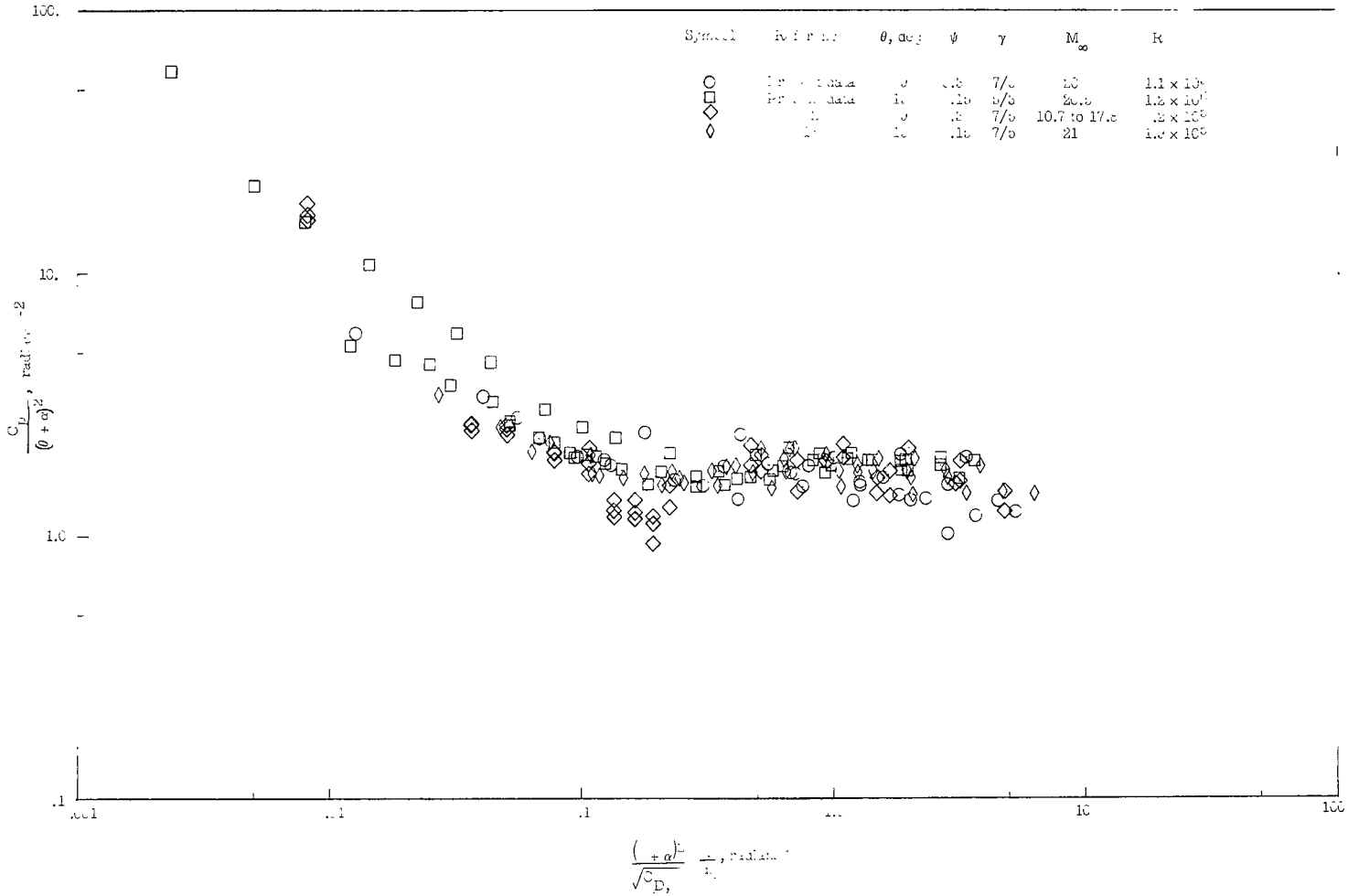

(b) $5^0 \leq \alpha \leq 40^0$.

Figure 8.- Concluded.

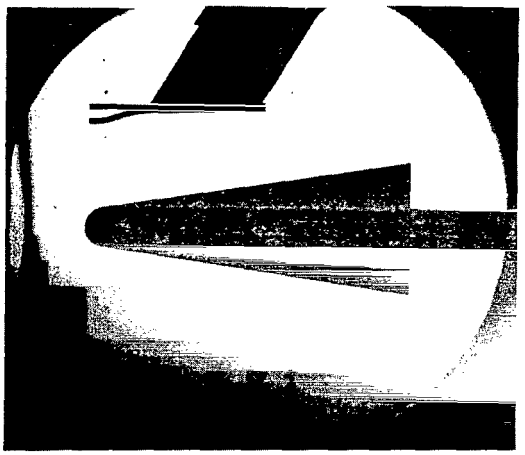

(a) 9^{o} spherically blunted cone; $\gamma = 7/5$; $R = 1.1 \times 10^{5}$.

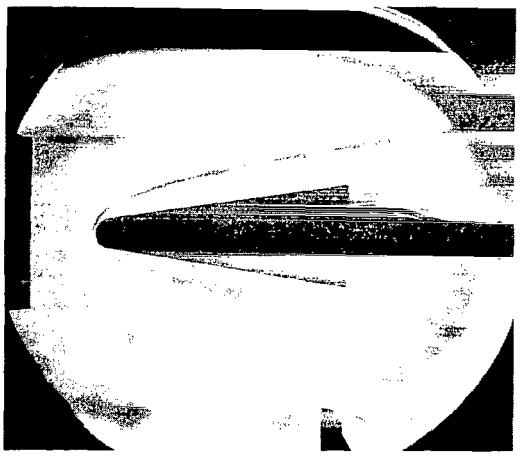

(b) 9^{o} spherically blunted cone; $\gamma = 5/3$; $R = 1.2 \times 10^{6}$.

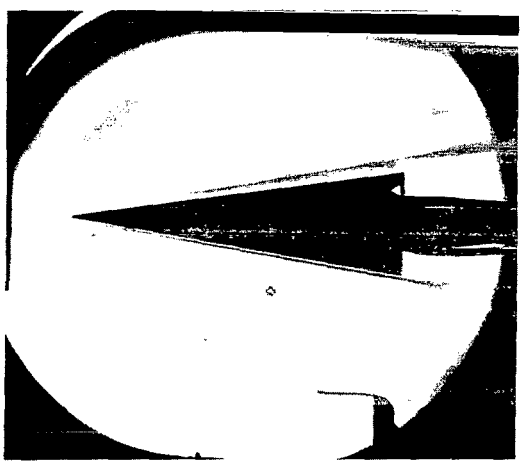

(c) 9^{o} flat-faced cone; $\gamma = 5/3$; $R = 1.2 \times 10^{6}$.

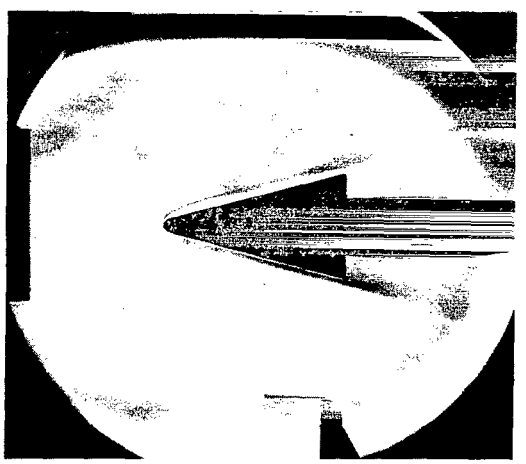

(d) 15^{o} spherically blunted cone; $\gamma = 5/3$; $R = 1.2 \times 10^{6}$.

Figure 9.- Representative schlieren photographs. $\alpha = 0^{o}$; $M_{\infty} \approx 20$. L-67-6673

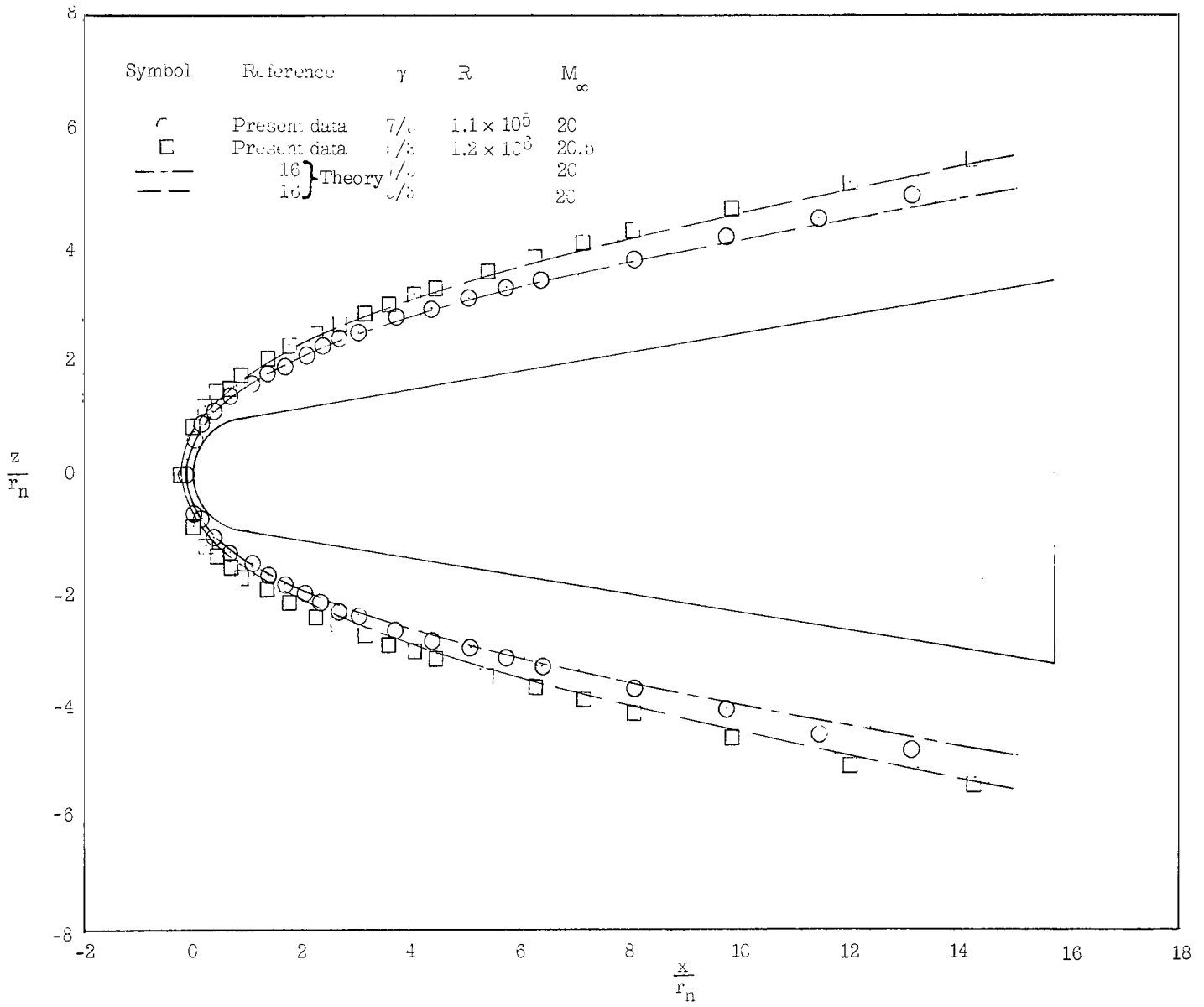

Figure 10.- Shock shapes in nitrogen and helium for a 9° spherically blunted cone. $M_\infty \approx 20$; $\alpha = 0^\circ$; $\psi = 0.3$.

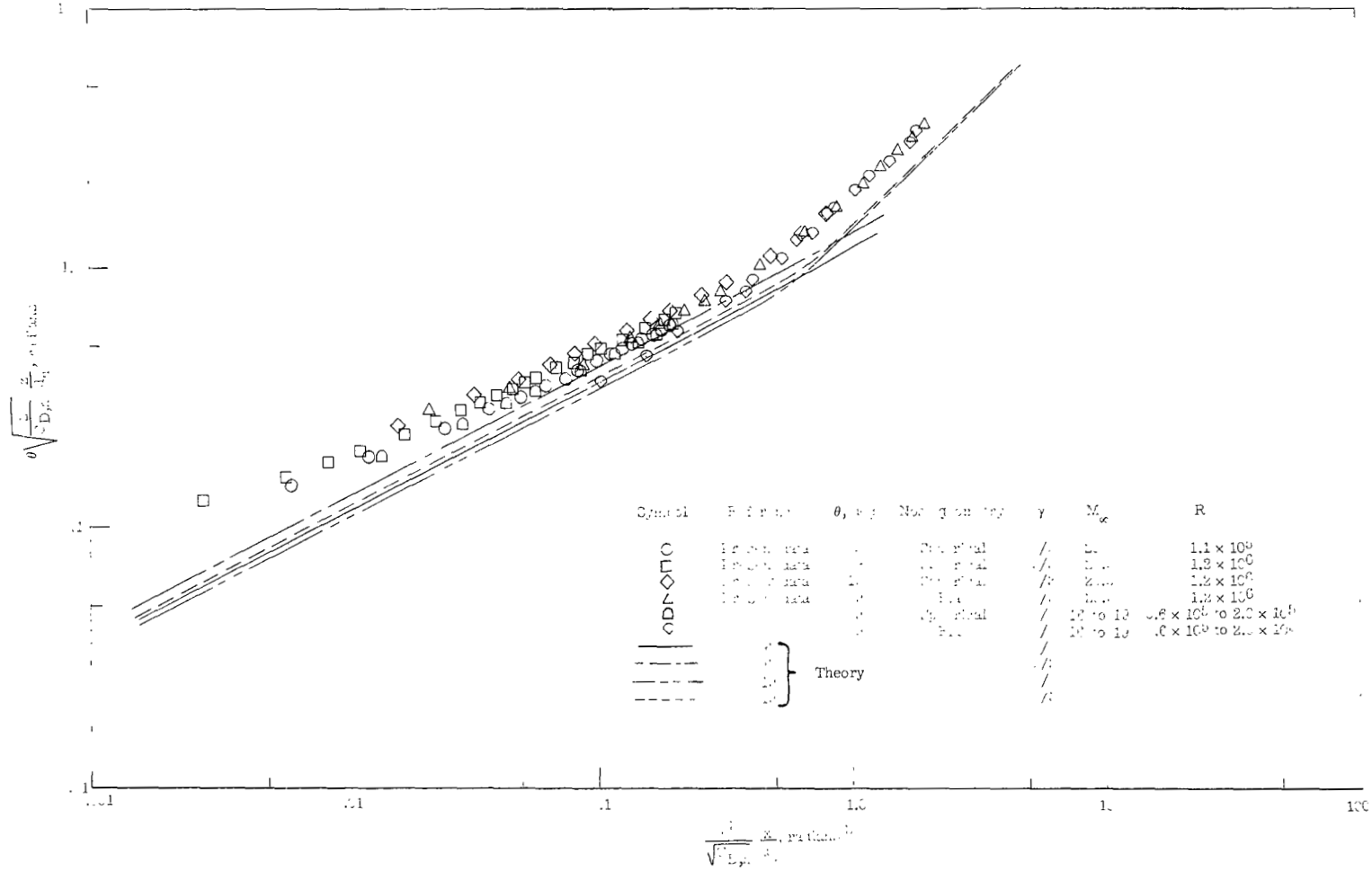

Figure 11.- Shock shape correlation for $\alpha = 0^0$.

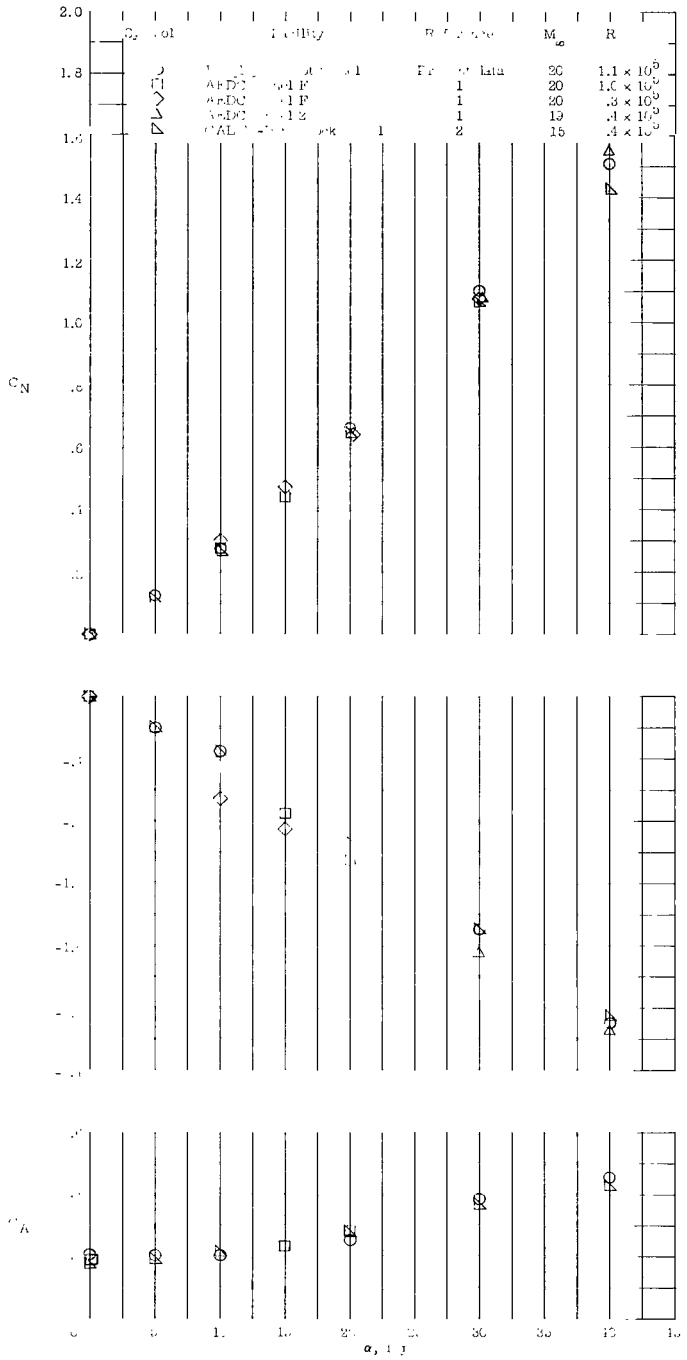

(a) Referred to body axis system.

Figure 12.- Longitudinal aerodynamic characteristics of a 9° spherically blunted cone. ψ = 0.3; r_b = 3.81 cm; γ = 7/5.

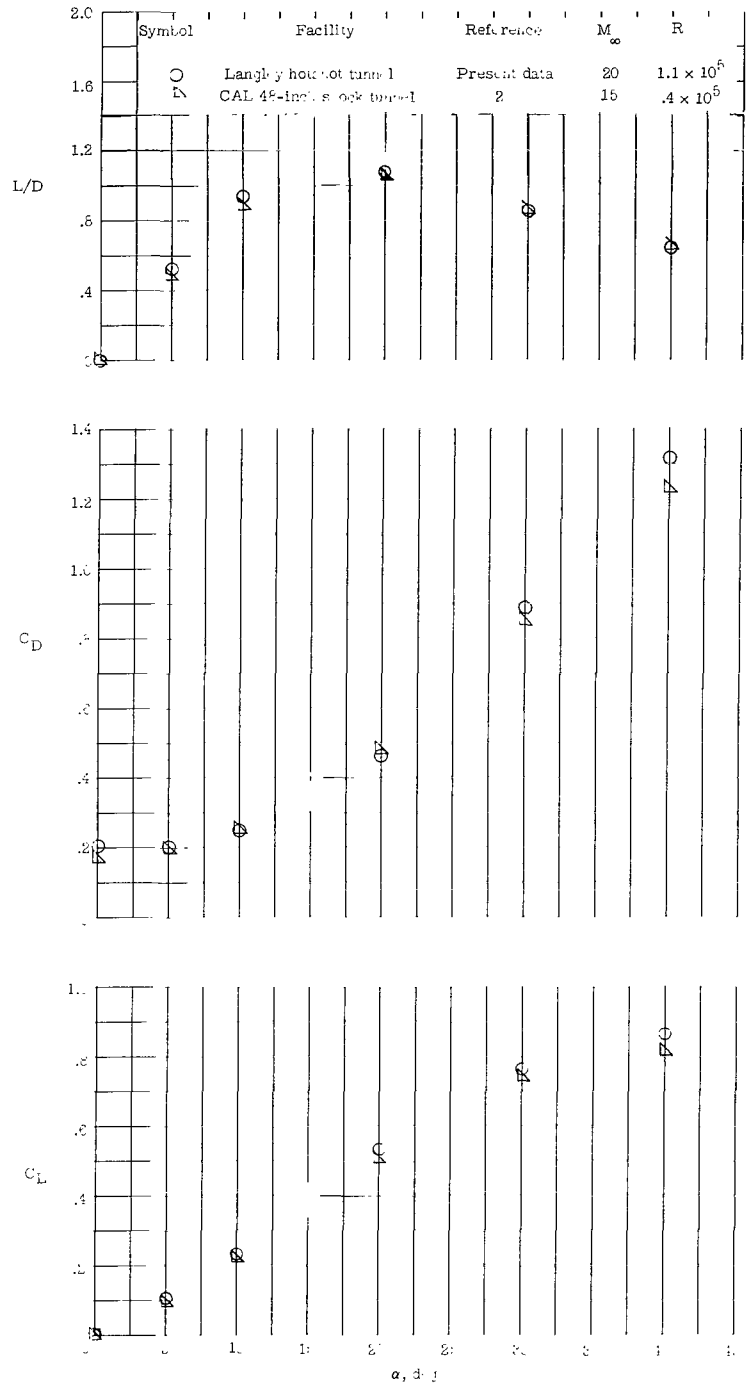

(b) Referred to stability axis system.

Figure 12.- Concluded.

NASA-Langley, 1968 —— 1 L-5392

"The aeronautical and space activities of the United States shall be conducted so as to contribute . . . to the expansion of human knowledge of phenomena in the atmosphere and space. The Administration shall provide for the widest practicable and appropriate dissemination of information concerning its activities and the results thereof."

—NATIONAL AERONAUTICS AND SPACE ACT OF 1958

NASA SCIENTIFIC AND TECHNICAL PUBLICATIONS

TECHNICAL REPORTS: Scientific and technical information considered important, complete, and a lasting contribution to existing knowledge.

TECHNICAL NOTES: Information less broad in scope but nevertheless of importance as a contribution to existing knowledge.

TECHNICAL MEMORANDUMS: Information receiving limited distribution because of preliminary data, security classification, or other reasons.

CONTRACTOR REPORTS: Scientific and technical information generated under a NASA contract or grant and considered an important contribution to existing knowledge.

TECHNICAL TRANSLATIONS: Information published in a foreign language considered to merit NASA distribution in English.

SPECIAL PUBLICATIONS: Information derived from or of value to NASA activities. Publications include conference proceedings, monographs, data compilations, handbooks, sourcebooks, and special bibliographies.

TECHNOLOGY UTILIZATION PUBLICATIONS: Information on technology used by NASA that may be of particular interest in commercial and other non-aerospace applications. Publications include Tech Briefs, Technology Utilization Reports and Notes, and Technology Surveys.

Details on the availability of these publications may be obtained from:

SCIENTIFIC AND TECHNICAL INFORMATION DIVISION

NATIONAL AERONAUTICS AND SPACE ADMINISTRATION

Washington, D.C. 20546